THE ANALYSIS OF NERVE AND MUSCLE ELECTRICAL WAVEFORMS WITH THE FAST FOURIER TRANSFORM AND CORRELATION TECHNIQUES

by

CHARLES HOWARD HIGHTOWER

B. S., Kansas State University, 1966

A MASTER'S THESIS

submitted in partial fulfillment of the

requirements for the degree

MASTER OF SCIENCE

Department of Electrical Engineering

KANSAS STATE UNIVERSITY
Manhattan, Kansas

1968

Approved by:

Donald H. Lenhert
Major Professor

TABLE OF CONTENTS

CHAPTER I

INTRODUCTION

1.1 Motivation and General Purpose

This thesis is concerned with the regulation of respiratory muscles in animals. The living organism is a complex structure with many degrees of freedom and whose operation is nonlinear and nonstationary. The deterministic behavior, if any, is usually hidden by stochastic variations. The ventilation system of any living organism is influenced by many factors. An excellent conceptualization was suggested by Goodman (1964) for the respiratory system of man. It is equally applicable to any living organism (Fig. 1.1).

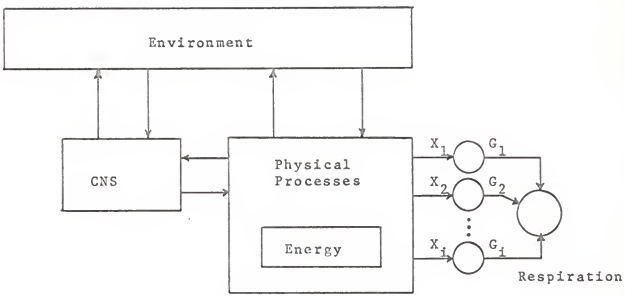

Fig. 1.1. Conceptual diagram showing manipulation of ventilation

The body is represented as an active system containing its own store of internally manipulated energy. Physical processes are coupled with the central nervous system and the environment. A finite number of state variables, e.g., blood oxygen tension, blood CO_2 content, body temperature, etc. indicated by X_1, X_2, ..., X_i are transformed by some unidentified dynamic operators G_1, G_2, ..., G_i and their superimposed effects produce the manipulation of ventilation. Ideally, knowledge of the dynamic operators G_1, G_2, ..., G_i in conjunction with the state of the animal would enable the complete prediction of the organism's respiratory behavior.

The purpose of this thesis evolved from research currently underway in the Department of Physiology at Kansas State University. Physiologists are investigating chemoreceptors associated with the CO_2 sensing mechanism of the chicken. These chemoreceptors sense the blood CO_2 tension and stimulate the neuro-muscular system to adjust the respiratory amplitude to compensate for the variation in blood CO_2 tension. The close relationship between a dynamic operator of Fig. 1.1 and these chemoreceptors is obvious. Experimental data consisted of electrical waveforms recorded from within the chicken respiratory system for controlled levels of blood CO_2 tension.

Based on the close relationship between a dynamic operator and the CO_2 chemoreceptors it was asked whether a model accounting for the effect of the CO_2 chemoreceptors on respiratory electrical activity could be constructed. Such a model would

lead to the explicit definition of at least one dynamic operator in Fig. 1.1 for the chicken. Experience and knowledge obtained from the chicken (a rather primitive organism) would, it is hoped, be a stepping stone to the understanding of the vital process of respiration and body functioning in higher animals, including man.

This thesis presents the results of an effort to illuminate the relationship between the CO_2 chemoreceptors and respiratory electrical activity through an analysis of the respiratory electrical activity for controlled levels of CO_2 in the chicken. In addition, a mathematical model of the respiratory system is constructed and a function dependent on only the system parameters and state of the chemoreceptors is derived.

It is hoped that the results of this work will be carried on until all the dynamic operators associated with respiration are discovered and the conceptual diagram of the respiratory system as shown in Fig. 1.1 is completely described.

1.2 Summary of Chapter Development

Chapter II begins the study of the observed CO_2 chemoreceptors effect on the nerve and muscle electrical activity with a brief introduction to the physiological processes involved in respiration. Topics include the generation of electrical behavior and the observed effect of CO_2 on the respiratory system.

A model of the respiratory system comprises the substance of Chapter III. A fairly detailed description of the laboratory experiment is presented in Chapter IV. A block diagram of the recording system is also included in Chapter IV.

Chapter V defines the mathematical functions that are pertinent in studies of respiratory electrical behavior. The cross correlation function is shown to be a measure of system model accuracy in this chapter. The subject of Chapter VI is the effect of digitizing the experiment analog signals and the effects of aliasing due to a sampling rate below the Nyquist frequency. The Fast Fourier Transform is also discussed.

The results and conclusions based on computer processing are included in Chapter VII. In addition, at the back of this thesis are included two appendices, Appendix A is a description of the digital processing system designed for the data processing required by this thesis. Appendix B is a mathematical analysis that is used to derive part of the results of Sec. 5.8.

CHAPTER II

DESCRIPTION OF PHYSIOLOGICAL PROCESSES INVOLVED IN RESPIRATION

2.1 The Nervous System

In order to describe the physiological processes that enter into the nerve and muscle processes leading to respiration, a history of a nerve signal will be traced as it is conducted along a fiber, traverses a synapse and becomes integrated with other electrical activity, and finally participating in the firing of a muscle fiber.

2.1.1 Conduction in Fibers

It is convenient to compare neural activity to an electric circuit. The circuit carries messages (nerve signals) through wires (nerve fibers) to a load (muscle cells).

A major difference exists between the nervous system and the electrical analogy. A nerve fiber has the ability to propogate a signal throughout its length without attenuation. This is possible because energy is available to the nerve from properties associated with the chemical composition of the fluid surrounding and internal to the nerve fiber. Of course, this differs from a wire in an electrical circuit in which a transmitted signal is attenuated by the resistance of the wire.

A stimulus produced by a change in the animal's environment will cause a nerve impulse to be transmitted along the nerve. If the stimulus is above a certain threshold level, a pulse will be conducted along a fiber (axon). This is commonly referred to as the "all or none" law.

2.1.2 Electrical Phenomena Associated with Impulse Generator and Impulse Conduction

The transmembrane potential of a nerve cell (neuron) is due to the separation of charge across the membrane surrounding the neuroplasm of the nerve. The membrane of a resting nerve resists passage of sodium ions (Na^+), but potassium ions (K^+) and chloride ions (Cl^-) move more freely through the membrane. Outside the membrane there is a high concentration of Na^+ and Cl^- ions and a low concentration of K^+ ions, since the K^+ ion can move out of the cell along its concentration gradient more easily than Na^+ ion can move into the cell, there tends to be a slight excess of positively charged ions in the outside of the membrane.

When a resting nerve is stimulated above the threshold level, a wave of depolarization travels away from the point of stimulation. This wave involves an increased permeability of Na^+ ions through the membrane. This causes the inside of the cell to lose its normally negative charge and become positive. Furthermore, the region outside the membrane having lost Na^+ ions now is at a lower potential than the area still surrounded by Na^+ ions.

Immediately after depolarization occurs, repolarization begins as the result of an increased outward flow of K^+ ions. This reestablishes the separation of charge and hence the normal resting potential. However, the interior of the cell now has a few more Na^+ ions than it had before the depolarization and the extra cellular fluid now has a few more K^+ ions. Na^+ ions are actively transported from the interior of the nerve through the membrane to the fluid surrounding the nerve and the K^+ ions are actively transported to the interior of the cell. The original concentration gradient is then restored across the membrane.

2.1.3 Synaptic Junctions

The neuron is composed of three parts 1. dendrites, 2. body, and 3. axon. These are analogous to the inputs, network, and outputs of an electrical circuit. In this case the network is a simple additive type. The input to a neuron can consist of many pulses carried by axons originating from other neurons. The output of the neuron is the integrated effect of the input impulses and is directed towards other nerve cells or toward the muscle cells. Such a junction between two nerve cells is called a synaptic junction.

2.1.4 The Nerve-Muscle Junction

The end of a nerve leaving the spinal cord which is associated with respiration is in a respiratory muscle. The

electrical signals carried by the axons stop here and do not travel beyond the nerve ending. Instead, a chemical is liberated at the interface which depolarizes the muscle fibers. This depolarization in turn leads to contraction.

2.1.5 Electrical Action of Muscle Cells

When a muscle fiber is stimulated a chemical change occurs over its entire surface. The chemical change results in an external voltage potential in the region surrounding the cell.

2.2 Physical Description of the Respiratory System

The respiration system in the chicken differs from the respiratory system common to mammals. In the mammal, the rate of respiration directly affects the oxygen (O_2) and carbon dioxide (CO_2) partial pressures in the blood. A similar situation exists in the chicken. However, this condition can be suppressed surgically without drastically altering the chicken's normal body functions.

2.2.1 The Respiratory System

Fig. 2.1 is a simplified diagram illustrating the basic action and parts of the respiratory system of the chicken. The air sac can be imagined to operate as a fireplace bellows. As the chest muscles squeeze the air sac, air is forced out of the sac and through the air ducts. When the chest muscles expand the air sac, air rushes through the air ducts to fill the low pressure area created in the air sac.

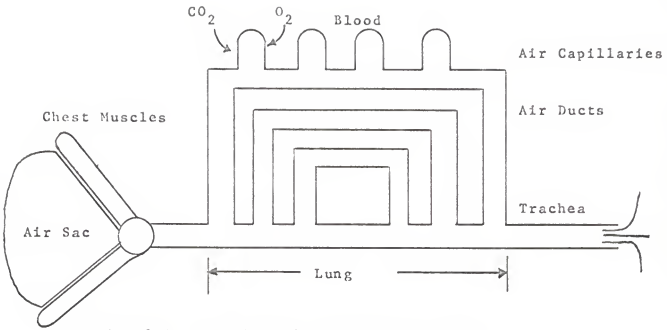

Fig. 2.1. Simplified respiratory system

As muscles cause the air sac to expand, air is drawn into the trachea. In the animal, the number of parallel air ducts is actually much greater than shown in the figure. Their combined passage area is much greater than the area of the direct path through the lung to the air sac so most of the inrushing air flows through the passage of least resistance, namely, the air ducts.

Gas diffuses into the diventricula of these parallel air ducts, called air capillaries. The exchange of O_2 and CO_2 occurs between the gas and the blood in the air capillaries. The efficiency of the system is increased by the unused air stored in the air sac. When the volume of the body decreases on expiration and gas is forced from the air sac, the unused gas located therein passes once more through the air ducts and is available for exchange a second time.

2.2.2 Modification of the Respiratory System to Enable Laboratory Control of Respiratory Movements

A mid-ventral incision from the chicken's trachea to its cloaca exposes the air sacs. The air sacs are then punctured with a sharp instrument. Inserting a tube into the trachea from an externally controlled gas source completes the operation (Fig. 2.3). Gas is then passed in a unidirectional manner into the trachea, through the lung, and out to the atmosphere through the hole in the air sacs. While this is done the animal is under deep anesthesia and has no sense of pain. If exposed tissues are kept moist with physiological saline the bird will live for many hours in this state. An excellent description of this surgical technique is given by DeWet (1966, pp. 250-263).

As the CO_2 chemoreceptor in the animal's body senses the CO_2 concentration of the gas being forced through its air ducts they respond by stimulating the central nervous system to manipulate the chest muscles in a manner which would normally cause the CO_2 level to return a normal value. With the air sacs punctured these efforts are futile because the bellows has a large hole in it. The steady stream of gas which is forced through the air ducts is unaffected by the movement of the chest muscles.

To increase the amplitude of respiration (i.e., magnitude of the movement of the chest muscles) it is only necessary to increase the percentage of CO_2 in the gas forced through the

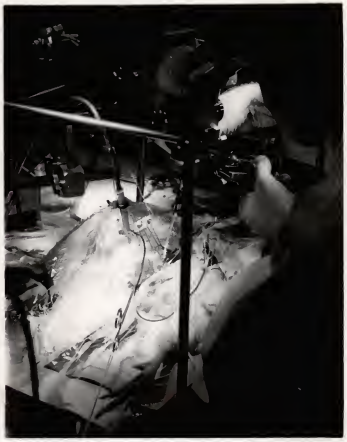

Fig. 2.2. Midventral incision in Gallus Domesticus showing position of recording electrodes

lungs. Decreasing the percentage of CO_2 in the ventilating gas produces the opposite reaction and respiratory movement is decreased. It is even possible to halt respiratory movement completely by eliminating the CO_2 from the input gas source.

CHAPTER III

A MODEL OF THE RESPIRATORY SYSTEM

3.1 A Model of the Respiratory Nerve-Muscle System

From the previous section involving the physiology of the chicken, a model representing the gross behavior of the respiratory system was constructed. It includes the three major elements of the system. Namely, the CO_2 sensing dynamic operator, the central nervous system, and the respiratory muscles. This model is shown in Fig. 3.1.

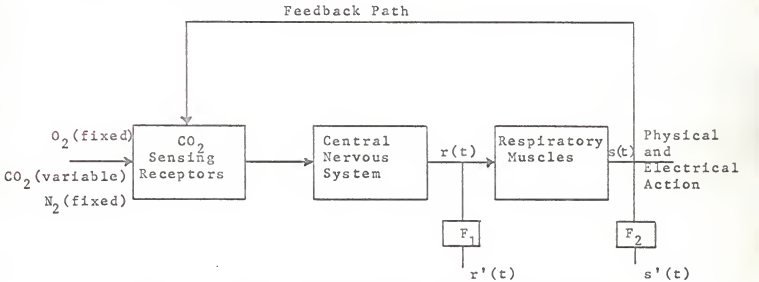

Fig. 3.1. Model of the chicken respiratory system including feedback and instrumentation effects

3.2 Explanation of the Model

The dynamic operator studied is represented by the first box. It contains the unknown dynamic operator that senses the inspired CO_2 level and triggers the nervous system to respond

appropriately. The central nervous system and its myriad of nerve bundles is represented by the second box. It is assumed to contain only those nerves associated with the respiratory system. The electrical signals carried by all the nerves are called collectively r(t).

The bird responds to the electrical signals of the nervous system by increasing or decreasing the contraction of its respiratory muscles. The muscles involved in this movement are represented by the third box. The muscles react to the stimulating electrical signals (Refer to Sec. 2.1.5) which are represented by s(t) in the model.

Ordinarily, the movement of the chest muscles causes an increase or decrease of CO_2 in the animal's blood. This causes the CO_2 sensing dynamic operator to change its state. This action is represented by the feedback loop from the muscle output to the CO_2 sensing chemoreceptors in Fig. 3.1.

F_1 and F_2 represent the bandwidth limitations imposed on the electrical activity by the recording instrumentation. The signals perturbed by instrumentation are called r'(t) and s'(t) for the perturbed nerve and muscle signals, respectively.

3.3 Limitation of the Model Associated with Constraints Imposed by Instrumentation

It is apparent that the compactness and delicate nature of the electrical probes used to record the animal's electrical activity limits the application of the model to a discrete

level of the overall respiratory system, mainly due to the fact that only the electrical activity of one nerve bundle can be recorded. Likewise, only the muscular activity from a small area near the recording electrode was recorded. It is hoped that the results of this sampling are applicable to generalizations about the entire system. However, this cannot be verified at this time.

CHAPTER IV

DESCRIPTION OF THE EXPERIMENT PERFORMED ON THE GALLUS DOMESTICUS

4.1 Introduction

Observation of the respiratory movements in the Gallus Domesticus (common chicken) shows that the respiratory muscles undergo a smooth, graded contraction. This is brought about by a host of complex properties, for example, muscle structure, membrane properties, patterns of innervation, and excitation-contraction coupling mechanisms. This section illustrates the techniques used to record electrical activity associated with the relationship of the CO_2 dynamic operator's state upon the electrical waveforms in the respiratory nerves and muscles under its control.

4.2 Method of Varying Nerve and Muscle Electrical Activity with Selected Levels of CO_2

The phenomenon studied was the influence of the dynamic operator as it manifested itself in the electrical waveforms of the respiratory nerve and muscle system for various levels of CO_2. Thus it was first necessary to prepare the animal for external control of the dynamic operator and respiratory rate as described in Sec. 2.2.2. The gas mixture forced through the trachea consisted of air supplied by a pressure vacuum air pump

and CO_2 supplied from a tank. These gases were metered with a floating ball meter for air and a differential pressure meter for CO_2. Since air contains very little CO_2, the CO_2 in the animals lungs was controlled by regulating the CO_2 from the tank.

The percentage of CO_2 varied the state of the respiratory muscles. When the percentage was low (below 3-6%) the animal ceased phasic contractions and exhibited no respiratory movement (state of apnea). When the percentage was elevated the animal began phasic respiratory movements which became progressively greater as the CO_2 level was increased. The levels of CO_2 used were 0%, 2%, 4%, 6%, 8%, 10%, 12%, and 14%.

4.3 Electrical Monitoring and Recording Apparatus

The recording equipment was substantially the same as used by De Wet (De Wet, 1966). The only modification was the addition of a Precision Instruments FM one channel tape recorder (Fig. 4.1). This recorder provided a time expansion-contraction capability. It was possible to record and playback at 37.5 ips and .375 ips respectively, without loss of frequency response.

Electrical recordings of efferent neural activity to a respiratory muscle were taken from a tiny isolated nerve branch of the 6th thoracic nerve. The nerve was cleaned of connective tissue and draped over a small pair of silver electrodes. The electrodes were attached to a cathode follower impedance matching amplifier and then into a high gain ac

amplifier. The amplifier output was parallel to one channel of a multichannel oscilloscope and to the normally closed position of a coax switch. The pole of the coax switch was connected to the FM recorder input (See Fig. 4.1).

Electrical activity from the respiratory muscle (M. Transversus Abdominis) was recorded with two small, flexible, teflon-coated, stainless steel electrodes. These electrodes were sharpened so they easily penetrated the muscle. The electrodes were attached to another impedance matching cathode follower and to another high gain ac amplifier. The amplifier output was parallel to the oscilloscope and to the normally open position on the coax switch.

Energizing the coax switch, switched the recorder input from the nerve electrodes to the muscle electrodes. The entire system was calibrated so that 80 μvolts at the electrodes corresponded to 1.4 volts output on the FM tape recorder. The entire recording system was located outside the wire screened operating room to minimize electrical noise from 60 Hz sources.

4.4 Recording Procedure

It was found that high levels of CO_2 stimulated the animal to the extent that his movements were great enough to tear out the carefully implanted electrodes. Thus it was decided to begin recording nerve and muscle activity for high CO_2 levels and then decrease to lower levels. This allowed the critical stimulation point to occur when the animal was under maximum anesthesia.

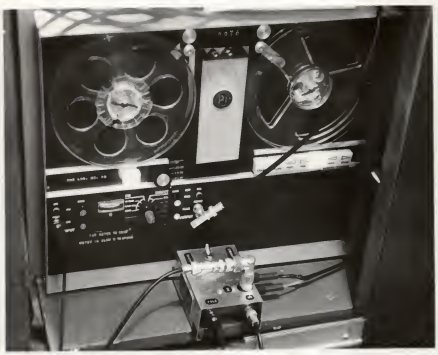

Fig. 4.1. FM recorder and coax switch used to record nerve and muscle electrical activity

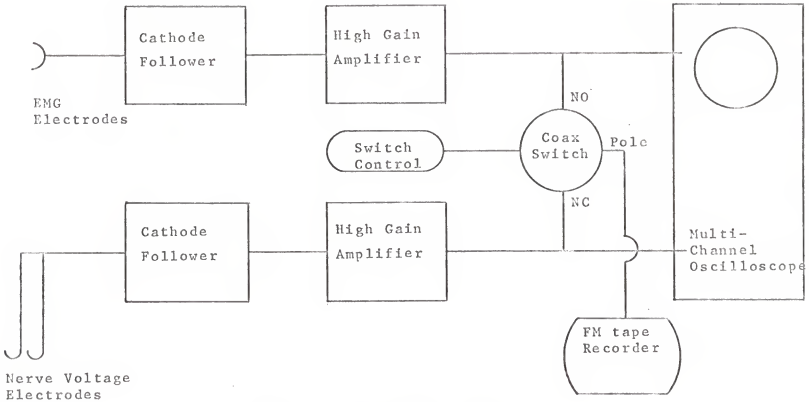

Fig. 4.2. Recording system

Ten seconds of nerve electrical activity were recorded immediately followed by ten seconds of muscle electrical activity for CO_2 levels of 14%, 12%, 10%, 8%, 6%, 4%, 2%, and 0% in that order. After the CO_2 level was changed each time, a delay of three minutes before recording was maintained to let the animal adjust completely to the new CO_2 level.

4.5 Brief Description of Data Processing System

Appendix A contains a detailed discussion and explanation of the analog-to-digital data processing system designed and developed for use in biomedical research at Kansas State University. The following sections serve to illuminate the process applied to the experimental data, recorded as previously described in order for it to be analyzed by a digital computer.

Basically, the processing system samples and quantizes analog data into a digital format suitable for computer input. The maximum sample and quantitization rate is 50 samples per second. This rate is usually sufficient for most biomedical data (e.g., electrocardiograms, fetal heartbeats, finger twitch, etc.). Higher sample and quantizing rates can be achieved by time expansion techniques (Refer to Sec. 6.1).

The data processing system consisted of an analog-to-digital convertor (ADC) and a digital stepping recorder (DSR) both under the control of a small general purpose computer. The ADC was manufactured by Texas Instruments and is discussed

in Sec. A.2. Digi-Data Corporation produced the DSR which is discussed in Sec. A.3. The general purpose computer was built by Remington-Rand. The computer and the machine language programs used in the control process can be found in Sec. A.5.

4.5.1 Creation of a Digital Magnetic Tape Containing Biomedical Data

The general purpose computer (Athena) controlled the sampling and recording equipment only. It performed no data analysis. Analysis was done later with the IBM 360/50 computer using the magnetic tape generated by the Athena controlled processing system. Operation of the sampling and quantitization system began with Athena addressing a selected analog input channel on the ADC. Quantitization of a 40 μsec. portion of the analog signal was done automatically by the ADC 1.5 μsec. after receiving the channel address command from the computer.

The 14 bit ADC output, in offset binary code, was then stored in the 256 twenty-four bit word core of the computer. The computer then placed the digitized sample and channel address at the DSR input where it was recorded on magnetic tape in a specified code (See Fig. A.8). This sequence occurred every 5 μsec., yielding a real-time sampling rate of 50 samples per second.

4.5.2 Decoding of the Coded Biomedical Data by the IBM 360/50 Computer

The magnetic tape produced by the data processing system containing experimental data was not in a standard IBM code (e.g., BCD, EBCIDEC, etc.). Therefore, further processing was required on the data before a useful analysis could be made.

The magnetic tape units associated with the IBM 360/50 have a capability of reading binary data into core without translation. Fig. A.9 (Appendix A) illustrates the way eight seven track tape characters were located in core bytes after such a read occurred on binary data without translation. Fig. A.11 is a flow chart of an assembler language program that converted the binary data in core back to a form differing from the measured voltage by only a scale factor. The assembler program writes the converted data on a nine track tape unit. The nine-track tape was then called by a standard Fortran IV program which multiplied by the scale factor and located the data once more in core but with the proper format for computer analysis.

CHAPTER V

DEFINING THE MATHEMATICAL FUNCTIONS PERTINENT TO THE ANALYSIS OF THE RECORDED ELECTRICAL ACTIVITY

5.1 Introduction

The mathematical functions that were thought to be significant in the study of nerve and muscle electrical activity are defined in this chpater. Although not all were used in this thesis, it is felt that defining them here will serve to benefit future work in this area. An analysis of a mathematical model of the respiratory system is presented in Sec. 5.8.1. The mathematical function used mainly in the subsequent analysis of the electrical activity was the Fourier transform and the associated power amplitude spectrum. The reason for not using the remaining functions was two fold. One, computer computation time exceeded reasonable limits. Two, the significance of the crosscorrelation function for two waveforms not recorded simultaneously yields little information of value if their similarity at the same time is to be studied. The mathematical functions of interest are:

1. the Fourier Series Amplitude-Frequency Plot
2. the Fourier Series Phase-Frequency Plot
3. the Fourier Integral
4. the Crosscorrelation Function
5. the Fourier Frequency Plots of the Crosscorrelation Function.

5.2 The Fourier Series

If a function f(t) is a periodic function of time with period T, it may be expressed as a Fourier Series as in Schwartz (1959, pp. 21-23) by,

$$f(t) = \frac{a_o}{T} + \frac{2}{T} \sum_{n=1}^{\infty} (a_n \cos\omega_n t + b_n \sin\omega_n t) \tag{5.1}$$

$$\text{where, } \omega_n = \frac{2\pi n}{T} \quad .$$

The coefficients a_n and b_n are found through the equations,

$$a_n = \int_{-T/2}^{T/2} f(t) \cos\omega_n t \, dt \qquad n=0, 1, \ldots \tag{5.2a}$$

$$b_n = \int_{-T/2}^{T/2} f(t) \sin\omega_n t \, dt \qquad n=1, 2, \ldots \tag{5.2b}$$

5.3 The Amplitude-Frequency Plot

The amplitude-frequency plot is proportional to a plot of $\sqrt{a_n^2+b_n^2}$ versus ω_n. Often this plot is referred to as the amplitude spectrum of the function f(t).

5.4 The Phase-Frequency Characteristic Plot

The phase-frequency characteristic plot is a plot of $\tan(-b_n/a_n)$ versus ω_n.

5.5 Complex Exponential Fourier Series Form

This is an alternative form of the Fourier series written as,

$$f(t) = \frac{a_o}{T} + \frac{2}{T} \sum_{n=1}^{\infty} C_n \cos(\omega_n t + \theta_n) \tag{5.3}$$

where, $C_n = \sqrt{a_n^2 + b_n^2}$

$\theta_n = \tan^{-1}(-b_n/a_n)$

$\omega_n = \frac{2\pi n}{T}$

5.6 The Fourier Transform

If a function is not periodic the Fourier series definition of Eq. 5.1 is not applicable. Examples of nonperiodic functions are transient responses and unit impulse responses. A Fourier transform can be defined for this case by the equation,

$$F(j\omega) = \int_{-\infty}^{\infty} f(t) e^{-j\omega t} dt \tag{5.4a}$$

and the corresponding time function can be recovered from $F(j\omega)$ with the equation,

$$f(t) = \frac{1}{2\pi} \int_{-\infty}^{\infty} F(j\omega) e^{j\omega t} d\omega \tag{5.4b}$$

provided, $\int_{-\infty}^{\infty} |f(t)|dt$ is finite.

5.7 The Crosscorrelation Function

If $f_1(t)$ and $f_2(t)$ are different periodic functions of the same fundamental frequency, the crosscorrelation function of these functions is defined in Lee (1960, pp. 17-18) as,

$$\Phi_{12}(\tau) = \frac{1}{T} \int_{-T/2}^{T/2} f_1(t)\ f_2(t+\tau)dt \tag{5.5a}$$

where, T is the period of $f_1(t)$ and $f_2(t)$

τ is the time displacement.

For aperiodic functions, the crosscorrelation function is defined as,

$$\Phi_{12}(\tau) = \int_{-\infty}^{\infty} f_1(t)\ f_2(t+\tau)dt \tag{5.5b}$$

where $f_1(t)$ and or $f_2(t)$ are aperiodic.

5.8 Fourier Series of the Crosscorrelation Function

Writing the Fourier series of $f_1(t)$ and $f_2(t)$ of period T as,

$$f_1(t) = \frac{a_{10}}{T} + \frac{2}{T} \sum_{n=1}^{\infty} C_{1n} \cos(\omega_n t+\theta_{1n}) \tag{5.6}$$

$$f_2(t) = \frac{a_{20}}{T} + \frac{2}{T} \sum_{n=1}^{n} C_{2n} \cos(\omega_n t+\theta_{2n}) \tag{5.7}$$

and $\omega_n = \frac{2\pi n}{T}$

enables the Fourier series of the crosscorrelation function to take the form,

$$\Phi_{12}(\tau) = \frac{a_{10}a_{20}}{T^2} + \frac{2}{T^2} \sum_{n=1}^{\infty} C_{1n}C_{2n} \cos(\omega_n\tau+\theta_{2n}-\theta_{1n}) \qquad (5.8)$$

where, $C_{jn} = \sqrt{a_{jn}^2+b_{jn}^2}$

$$\theta_{jn} = \tan^{-1}(-b_{jn}/a_{jn}) \quad . \qquad (5.9)$$

5.8.1 The Amplitude-Frequency Plot of the Crosscorrelation Function

The amplitude-frequency plot of $\Phi_{12}(\tau)$ is a plot of $C_{1n}\ C_{2n}$ versus ω_n. In terms of the original time functions this is a plot of $\sqrt{a_{1n}^2+b_{1n}^2} \cdot \sqrt{a_{2n}^2+b_{2n}^2}$ versus ω_n. As a consequence, if the average term or any harmonic is absent in either $f_1(t)$ or $f_2(t)$, the constant term or the corresponding harmonic term will be absent in the Fourier series of the crosscorrelation function.

5.8.2 The Phase-Frequency Plot of the Crosscorrelation Function

The phase-frequency plot of the crosscorrelation function is a plot of $\theta_{2n}-\theta_{1n}$ versus ω_n. In terms of the original functions this is a plot of the difference in phase between $f_1(t)$ and $f_2(t)$ versus ω_n.

5.8.3 A Mathematical Analysis of the Respiratory System Under Open Loop Conditions

The purpose of the following analysis is to demonstrate the applicability of the previously defined mathematical functions to the respiratory system model of Sec. 3.1 when the feedback loop is broken as described in Sec. 2.2.2. The analysis presented is a calculation of the crosscorrelation function between the nerve and muscle electrical waveforms. The crosscorrelation function was chosen because both the nerve and muscle signals are available simultaneously to the researcher so that the nerve-muscle crosscorrelation function computed with experimental data can be used as a check against the same crosscorrelation function derived from a mathematical model of the respiratory system.

The following analysis yields an equation relating the block diagram components $h_1(t)$, $h_2(t)$, and fpp(t) to the nerve-muscle crosscorrelation function. Interpretation of this equation reveals that the crosscorrelation function is suitable for use as a gauge to the accuracy of respiratory system models.

In Fig. 5.1 the signal received by the central nervous system from the CO_2 dynamic operator is labeled fpp(t). The affect of the central nervous system on fpp(t) is represented by $h_1(t)$, where $h_1(t)$ is the linear impulse response of the central nervous system. The nerve electrical activity s(t) is shaped by $h_2(t)$ to produce the muscle electrical activity r(t). It is assumed that $h_2(t)$ is the linear impulse response of the muscle system.

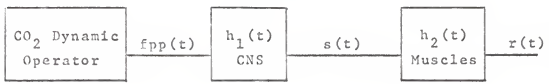

Fig. 5.1. Mathematical model of the respiratory system under open loop conditions

5.8.4 Derivation of the Nerve-Muscle Crosscorrelation Function

Due to the phasic nature of the respiratory electrical activity the crosscorrelation defining equation for periodic functions is used in this analysis. The crosscorrelation between r(t) and s(t), both of period T is written as

$$\Phi_{rs}(\tau) = \frac{1}{2T} \int_{-T}^{T} r(t)\ s(t+\tau)dt \quad , \tag{5.10}$$

where $\Phi_{rs}(\tau)$ is the nerve-muscle crosscorrelation function.

Because the nerve and muscle impulse response functions $h_1(t)$ and $h_2(t)$ were assumed to be linear, r(t) and s(t) can be written in terms of the following convolution integrals

$$r(t) = \int_{-\infty}^{\infty} h_2(\nu)\ s(t-\nu)d\nu \quad , \tag{5.11}$$

and,

$$s(t) = \int_{-\infty}^{\infty} h_1(\sigma) fpp(t-\sigma)d\sigma \quad , \tag{5.12}$$

where ν and σ are dummy variables. Direct substitution of Eqs.

5.11 and 5.12 into Eq. 5.10 yields for the crosscorrelation function,

$$\Phi_{rs}(\tau)=\frac{1}{2T}\int_{-T}^{T}\int_{-\infty}^{\infty}h_2(\nu)s(t-\nu)d\nu\int_{-\infty}^{\infty}h_1(\sigma)fpp(t+\tau-\sigma)d\sigma dt \quad . \quad (5.13)$$

Defining,

$$\Phi_{sf}(\tau+\nu-\sigma)=\frac{1}{2T}\int_{-T}^{T}s(t-\nu)fpp(t+\tau-\sigma)dt \quad , \quad (5.14)$$

Eq. 5.13 becomes,

$$\Phi_{rs}(\tau)=\int_{-\infty}^{\infty}\int_{-\infty}^{\infty}h_2(\nu)h_1(\sigma)\Phi_{sf}(\tau+\nu-\sigma)\,d\nu d\sigma \quad . \quad (5.15)$$

Eq. 5.16 can be manipulated so that,

$$\Phi_{rs}(\tau)=\int_{-\infty}^{\infty}h_2(\nu)\left[\int_{-\infty}^{\infty}h_1(\sigma)\Phi_{sf}(\tau+\nu-\sigma)d\sigma\right]d\nu \quad , \quad (5.16)$$

where the quantity in brackets is recognized as the convolution of the impulse response $h_1(t)$ with the crosscorrelation function of the CO_2 operator waveform fpp(t) and the nerve waveform s(t).

Using the symbol * to indicate convolution, Eq. 5.16 can be written as,

$$\Phi_{rs}(\tau) = \int_{-\infty}^{\infty}h_2(\nu)h_1(\sigma)*\Phi_{sf}(\tau+\nu-\sigma)d\nu \quad . \quad (5.17)$$

The variables associated with the convolution result in Eq. 5.17 are τ and ν. With this fact Eq. 5.17 is recognized as the aperiodic form of the crosscorrelation function of the impulse response $h_2(t)$ and the convolution result indicated in Eq. 5.17. Therefore Eq. 5.17 can be expressed as,

$$\phi_{rs}(\tau) = h_2(t) \ominus [h_1(t) * \phi_{sf}(\tau)] \quad , \tag{5.18}$$

where the symbol $\ominus$ means aperiodic correlation and * indicates convolution

This equation can be expanded further by writing $\phi_{sf}(\tau)$ in terms of the block diagram components. Pursuing this course, $\phi_{fs}(\tau)$ by definition is,

$$\phi_{fs}(\tau) = \frac{1}{2T} \int_{-T}^{T} s(t) fpp(t+\tau) dt \tag{5.19}$$

Substitution of Eq. 5.12 into Eq. 5.19 for s(t) results in the equation,

$$\phi_{sf}(\tau) = \frac{1}{2T} \int_{-T}^{T} \int_{-\infty}^{\infty} h_1(\alpha) fpp(t-\alpha) d\alpha fpp(t+\tau) dt \quad , \tag{5.20}$$

which can be reduced easily to,

$$\phi_{sf}(\tau) = \int_{-\infty}^{\infty} h_1(\alpha) \phi_{ff}(\tau+\alpha) d\alpha \quad , \tag{5.21}$$

where,

$$\phi_{ff}(\tau) = \frac{1}{2T} \int_{-T}^{T} fpp(t) fpp(t+\tau) dt \quad .$$

In terms of the previous notation for aperiodic correlation, Eq. 5.21 becomes,

$$\phi_{sf}(\tau) = h_1(t) \ \theta \ \phi_{ff}(\tau) \quad . \tag{5.22}$$

Upon substitution of this result into Eq. 5.18, the cross-correlation function of the nerve and muscle electrical activity is found to be,

$$\phi_{rs}(\tau) = h_2(t) \ \theta \ \{h_1(t) * [h_1(t) \ \theta \ \phi_{ff}(\tau)]\} \quad . \tag{5.23}$$

5.8.5 Comments on the Significance of the Nerve Muscle Crosscorrelation Function in Light of the Mathematical Analysis

It can be concluded from Eq. 5.23 that the crosscorrelation function of the nerve and muscle waveforms is solely dependent on the mathematical model system parameters and the autocorrelation function of the dynamic operator waveforms.

The operations called for by Eq. 5.23 are difficult to evaluate for any choice of $h_1(t)$, $h_2(t)$, or $\phi ff(\tau)$ even with a large digital computer. With the advent of the Fast Fourier transform (to be discussed) it is a relatively easy matter to compute the Fourier transform of Eq. 5.23 on a digital computer. Using the

results of Appendix B, the Fourier transform of $\Phi_{rs}(\tau)$ is

$$\Phi_{rs}(j\omega) = H_2(-j\omega)|H_1(j\omega)|^2 \Phi_{ff}(j\omega) \quad , \tag{5.24}$$

where $H_2(-j\omega)$ is the complex conjugate of the Fourier transform of $h_2(t)$, $|H_2(j\omega)|$ is the magnitude of the Fourier transform of $h_1(t)$ and $\Phi_{ff}(j\omega)$ is the power amplitude spectrum of the CO_2 dynamic operator waveform.

Thus it is concluded that modeling in the frequency domain of the respiratory system is the best method at present. Eq. 5.24 can be utilized as a guide to the accuracy of the model since the crosscorrelation function and its Fourier transform can be computed for real data and then compared to the results of Eq. 5.24.

Results of this mathematical analysis indicated that the study of the respiratory system begin in the direction of uncovering its characteristics in the frequency domain. This is the course of investigation that is followed throughout the remainder of this thesis.

CHAPTER VI

METHOD OF COMPUTER ANALYSIS

6.1 Introduction

Two animals were used in the experiment from which nerve and muscle activity was recorded for each level of CO_2 as stated in Sec. 4.4. Recording was done with a Precision Instruments FM recorder at a speed of 37.5 ips with a flat bandpass from 0Hz to 10 KHz. Selected protions of each signal at each CO_2 level were converted into digital form suitable for IBM 360/50 input by the data conversion system described in Appendix A. The data conversion system sampled the selected portions of the electrical signals 50 times/sec. To increase the effective sampling rate of the waveforms the FM recorder was slowed to a speed of .375 ips and its bandwidth reduced to 0Hz to 100Hz before processing by the data conversion system. This yielded an effective sampling rate on the original signals of 5000 samples/sec. The Nyquist sampling theorem states that bandlimited signals of finite energy with bandwidth f_c may be completely described from a knowledge of its samples taken at a rate of $2f_c$ per second (Landau, 1967). The highest possible frequency in the waveforms was 10,000 Hz due to the recorder bandpass filter. Thus a Nyquist sampling rate of 20,000 samples would be required for complete recovery. Since the sampling was done at a rate one-fourth as fast as the Nyquist frequency, there exists the possibility of aliasing

from high frequency components. This is discussed in the next section.

6.2 The Effect of Aliasing Due to a Sampling Rate Less That the Nyquist Frequency

A discussion of aliasing is given in Blackman and Tukey (1958) for a stationary random process which has been sampled at uniformly spaced intervals of time t viz,

$$t = 0, \Delta t, 2\Delta t, \ldots \quad .$$

Assuming that the signals in this thesis are at least stationary over the period of observation, a sampled waveform can be defined as

$$f_s(t) = \nabla(t;\Delta t)\ f(t) \quad , \tag{6.1}$$

where $f_s(t)$ is the sampled signal obtained from the analog signal f(t) by equispaced samples Δt secs. apart and $\nabla(t;\Delta t)$ represents an infinite dirac comb (Blackman and Tukey, 1958, p. 68) where,

$$\nabla(t;\Delta t) = \Delta t \sum_{n=-\infty}^{n=\infty} \delta(t-n\Delta t) \quad .$$

The Fourier transform of the analog signal is

$$F(f) = \frac{1}{T} \int_{-T/2}^{T/2} f(t)\ \exp(-j\omega t)dt \quad , \tag{6.2}$$

where F(f) is the real Fourier transform and $\omega = 2\pi f$.

The power amplitude spectrum corresponding to F(f) is simply,

$$P(f) = |F(f)|^2 \quad , \tag{6.3}$$

where P(f) is the power spectrum of the original time function f(t).

The Fourier transform of the sampled signal is given by

$$F_s(f) = \frac{1}{T} \int_{-T/2}^{T/2} f_s(t) \exp(-j\omega t) dt \quad , \tag{6.4}$$

where F(f) represents the Fourier transform of the discrete sampled function f(t). Substituting 6.1 into 6.2 yields

$$F_s(f) = \frac{1}{T} \int_{-T/2}^{T/2} \nabla(t;\Delta t) f(t) \exp(-j\omega t) dt \quad . \tag{6.5}$$

It is well known that the Fourier transform of a product can be obtained by convoluting the individual Fourier transforms in the frequency domain. Applying this fact to Eq. 6.5 yields the Fourier transform

$$F_s(f) = A(f;\frac{1}{\Delta t}) * P(f) \quad , \tag{6.6}$$

where $A(f;\frac{1}{\Delta t})$ is an infinite dirac comb in the frequency domain given by,

$$A(f;\frac{1}{\Delta t}) = \sum_{n=-\infty}^{n=+\infty} \delta(f-\frac{n}{\Delta t}) \quad ,$$

and * means convolution.

Eq. 6.6 can be expanded to,

$$F_s(f) = \sum_{n=-\infty}^{\infty} F(f-\frac{1}{\Delta t}) = F(f) + \sum_{n=-\infty}^{\infty} F(f-\frac{n}{\Delta t}); n\neq 0 \qquad (6.7)$$

Note that $F_s(f)$ differs from $F(f)$ by the terms,

$$\sum_{n=-\infty}^{\infty} F(f-\frac{n}{\Delta t}) \; ; \; n\neq 0$$

which are identical in shape to the actual Fourier transform, and centered on $n/\Delta t$. The effect of these additional terms on $F_s(f)$ is called aliasing since without them $F_s(f)$ would be identically $F(f)$ and hence $P_s(f)$ would equal $P(f)$.

Recognizing that $1/\Delta t$ is equal to the sampling frequency called f_s, then

$$fs = 5000 \text{ Hz}$$

for the data processing system.

Eq. 6.7 becomes,

$$F_s(f) = F(f) + \sum_{n=-\infty}^{\infty} F(f-nf_s); \; n\neq 0$$

for the data processing system. A little thought reveals that $F_s(f)$ is identical to $F(f)$ between 0 and $f_s/2$ Hz if the condition that no frequency components exist in $F(f)$ above $f_s/2$ is satisfied. Therefore, the data processing system can be expected to furnish a valid representation of the actual power amplitude plot up to $f_s/2$ or 2500 Hz only if there are no frequency components in the experimental waveforms above 2500 Hz.

The components in the recorded waveforms above 2500 Hz are small compared with the lower frequency components. A quantitative demonstration of this was done by filtering the experimental waveforms with high frequency cutoffs of 5000 Hz and 2500 Hz and observing the affects on the waveform. Only a slight affect on the waveform was observed for the 5000 Hz high frequency cutoff. It was noticed that a small rounding of the higher amplitude peaks occured in the waveform with a 5000 Hz high frequency cutoff. This rounding was more pronounced with a high frequency cutoff of 2500 Hz. No appreciable change in the waveform shape was observable with high frequency cutoffs of 20,000 Hz and 10,000 Hz.

Although these observations are not conclusive evidence for neglecting aliasing, they do lead to the acceptance of the calculated power spectra as being representative of the actual power spectra up to 2500 Hz. Furthermore, this analysis indicates that an effort to increase the sampling frequency by a factor of two (to 10,000 samples/sec) should be made. Qualitative evidence shows that this increased sampling rate would almost completely eliminate aliasing affects from the calculated power spectra.

6.3 The Fast Fourier Transform

Computer computation of the amplitude power spectra was done through an intermediate calculation of the Fourier transform coefficients. The relationship between the power amplitude spectrum and its associated Fourier transform is simply

$$P_n = a_n^2 + b_n^2$$

where P_n is the n^{th} amplitude of the power spectrum and a_n and b_n are the n^{th} Fourier coefficients.

Instead of using the defining equations to calculate a_n and b_n as given in Chapter 3, an algorithum was used called the fast Fourier transform (FFT) (Cochran, 1968). To use this algorithum as supplied in a Special Scientific Subroutine package supplied by IBM (IBM Ref. 8) it is necessary that the waveform to be Fourier transformed consist of 2N samples, where $2N = 2^m$ and m is a positive integer between 3 and 20.

The defining equation for the FFT is,

$$A_n = a_n + jb_n = \sum_{k=0}^{2N-1} x_K \exp(-2\pi jnk/N); \quad n=0, 1, \ldots, N-1,$$

where A_n is the complex n^{th} coefficient of the FFT and x_k denotes the k^{th} sample of the sampled time series.

If the original continuous waveform is considered bandlimited and sampled at the Nyquist rate it is possible to truncate the waveform after 2N samples and assume a periodic continuation of the 2N samples.

The Fourier coefficients of this series as computed by the FFT differ from the Fourier coefficients of the original bandlimited waveform only by an aliasing distortion.

The aliasing distortion was shown to be small in Sec. 6.2 so that the amplitude power spectra computed via the FFT should be a realistic approximation of the actual unaliased power spectra.

The greatest advantage in using the FFT is that it is highly efficient in computing the Fourier coefficients from a time-cost standpoint. If the time series consists of $N = 2^n$ samples then about $2N \log_2 N$ arithmetic operations will be required to evaluate all associated FFT coefficients. The number of operations required for conventional calculation of the Fourier coefficients requires at least N^2 operations. For example, in this thesis the FFT for N = 8192 samples was computed (i.e., n = 13), the sum of the squares of the coefficients computed, the results condensed, normalized, and plotted in 2.56 minutes. Typical results of the FFT applied to the nerve and muscle waveform for various CO_2 levels are shown in Fig. 7.1 and Fig. 7.2.

6.4 Crosscorrelation Function

Two factors were responsible for the negation of this calculation in this thesis. The first factor that served to eliminate calculating the crosscorrelation function between the nerve and muscle signals for various CO_2 levels was that such a computation required the nerve and muscle signals to be recorded simultaneously so that the CO_2 state was the same for both waveforms. The one channel recorder used in this experiment did not allow this.

Furthermore, the calculation of the crosscorrelation function by conventional means requires at least N^2 calculations. With data for 26 experiments, the time this would have

taken would exceed reasonable bounds. However, it is suggested that a limited number of crosscorrelation functions be computed in the future after modeling of the respiratory system has been done to check the validity of the model and a suitable two channel FM recorder is obtained.

CHAPTER VII

ANALYSIS OF THE NERVE AND MUSCLE POWER AMPLITUDE FREQUENCY PLOTS

7.1 Introduction

A respective normalized power spectrum is depicted in Fig. 7.1. It is typical of both the nerve and muscle power amplitude plots calculated by means of the FFT and plotted on the IBM 360/50 computer.

Note that P(f) is equal to zero at 500 Hz and 1000 Hz. It was necessary to set the power at these frequencies equal to zero since unusually large amplitudes appeared at these two frequencies. They were due to the carrier frequency oscillator in the FM tape recorder. The carrier frequency, at a tape speed of .375 ips, was 500 Hz. Theoretically the carrier frequency and any higher harmonics are eliminated by a 0 to 100 Hz bandpass filter built into the recorder. The Fourier coefficients of a sinusoid of frequency f_o have a very large amplitude concentrated at f_o in the power amplitude plot. Therefore, the coefficients corresponding to the FM recorder's carrier frequency and second harmonic predominated over the coefficients of the waveform at these frequencies.

These large values ruined the normalizing routine used in the plotting routine. Therefore, they were arbitrarily set to zero to eliminate this problem. Therefore, no physiological significance is associated with the lack of power at 500 and 1000 Hz.

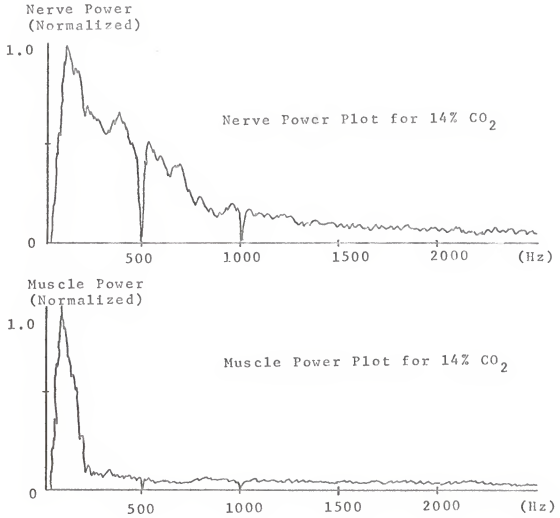

Fig. 7.1. Typical normalized power amplitude plots for nerve and muscle waveforms

From plots similar to Fig. 7.1 done for each nerve and muscle waveform a cumulative power plot was made (Fig. 7.2). The purpose of these being that the bandwidth of each signal could then be defined.

A white noise component was common to all the power spectra plots as indicated by the relatively constant amplitudes in Fig. 7.1 extending from 1000 Hz to 2500 Hz. This noise component was eliminated from the cumulative power spectra by a graphical technique. The bandwidth of a waveform was defined as that frequency below which 90% of the waveform's power was located after removal of white noise components. No frequency components appeared in any of the plots below 30 Hz because the high gain amplifier in the recording system had a low frequency cutoff of 35 Hz to eliminate artifact (e.g., body movement of probes, heartbeat, etc.) from the recorded waves.

Once the plots were compensated for the FM carrier oscillator energy and white noise perturbations, an investigation of the CO_2 dynamic operator state and its affect on the waveforms bandwidth and power content was initiated. The results of which are discussed in the next two sections.

7.2 The Effect of CO_2 Dynamic Operator State on the Muscle Waveform Power Spectra Characteristics

The two most apparent affects for various operator states were found to be the waveform's bandwidth and its relative power content. The relative power content was based on the amplitude

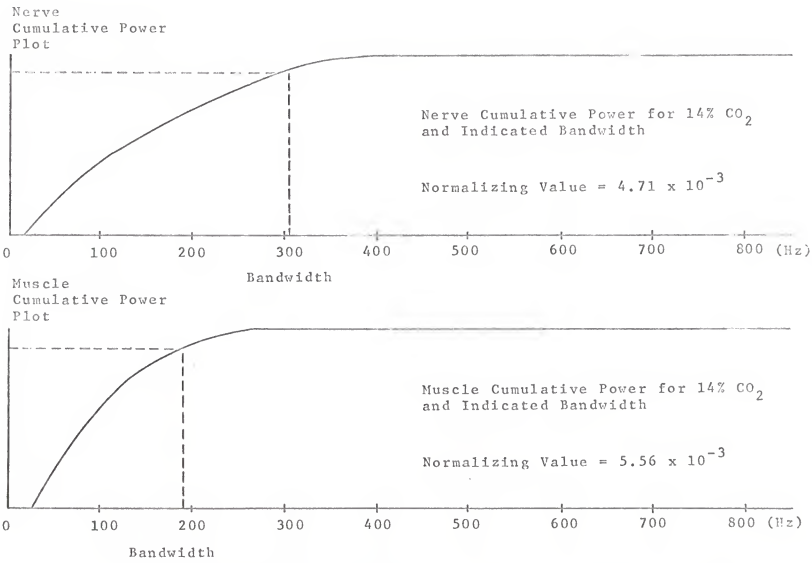

Fig. 7.2. Typical normalized cumulative power plots for nerve and muscle waveforms

of the cumulative power spectra at its horizontal asymtote (after accounting for normalization). The largest asymptote was defined as 100%.

The state of the dynamic operator was indicated by the measure of inspired CO_2. The results of bandwidth analysis are shown in Fig. 7.3. Fig. 7.3 graphically illustrates how the CO_2 level affected the muscle waveform bandwidths in the experiment. No bandwidth values appear below 6% CO_2 because all muscle action ceased and the associated electrical activity was not great enough to be distinguished from noise in the recording system.

Fig. 7.3 indicated that decreasing levels of CO_2 still maintaining phasic respiratory movement, produce an almost linear decrease in muscle waveform bandwidth. In Fig. 7.3, changing the state of the operator from 14% CO_2 to 10% CO_2 caused a corresponding decrease of bandwidth from 194 Hz to 153 Hz.

At a level of 8% CO_2, the animal was observed to be approaching apnea. When this occurred, Fig. 7.3 indicated a comparitively large bandwidth (217 Hz). At 6% CO_2 the muscle bandwidth decreased to 177 Hz and below 6% CO_2 no muscle waveform was observable.

Fig. 7.4 is a plot of the relative power of each muscle waveform versus CO_2 level. It is observed that the relative power decreased as the CO_2 level decreased.

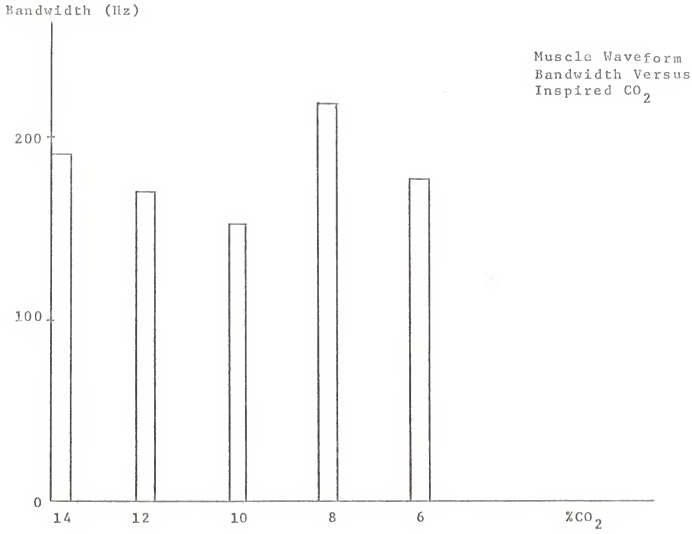

Fig. 7.3. Dynamic operator and its effect on muscle waveform bandwidth

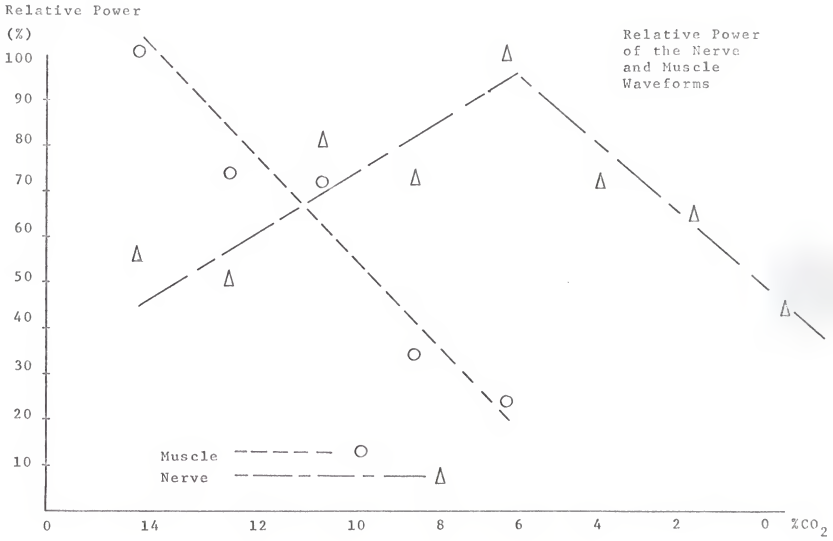

Fig. 7.4. Waveform relative power versus $\%CO_2$

7.3 The Effect of CO_2 Dynamic Operator State on the Nerve Waveform Power Spectra Characteristics

Results of the adjusted cumulative power spectra plots are summarized in Fig. 7.5 for the nerve waveform. The bandwidth is plotted as a function of the inspired CO_2 level. Decreasing CO_2 levels have an entirely different affect on the nerve waveform bandwidth than they did on the muscle waveform bandwidth (at least during phasic respiration).

Notably, as the CO_2 level decreased from 14% to 10% the nerve bandwidth remained practically constant. The bandwidths were 311 Hz, 321 Hz, and 316 Hz corresponding to CO_2 levels of 14%, 12% and 10% respectively.

Fig. 7.4 indicates that as the CO_2 level decreased from 14% to 10%, the relative power in the nerve waveform displayed a rising trend. The rising trend is diametrically opposite to the decrease in relative power displayed by the muscle waveform for the same CO_2 levels.

Again, as a state of apnea was approached (8% CO_2) a dramatic change in the power characteristics of the nerve waveform transpired. Abruptly, both the bandwidth and relative power increased to near maximum values at the onset of apnea. The relative power reached a maximum at 6% CO_2. Maximum bandwidth (817 Hz) occurred during apnea at a CO_2 level of 4%.

CO_2 levels of 2% and 0% displayed a decreasing trend in both the nerve waveform bandwidth and relative power. Notice that at low levels of CO_2 during which no respiratory muscle

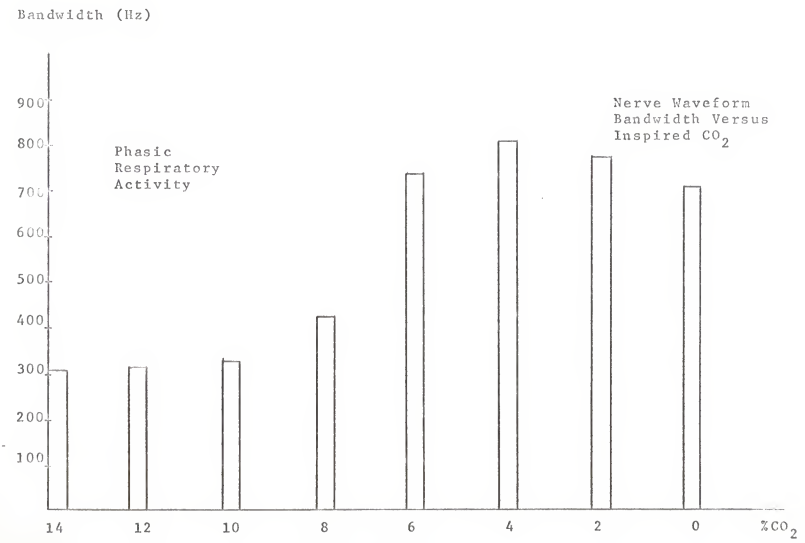

Fig. 7.5. Nerve bandwidth for various CO_2 levels

action existed there was still quite a bit of electrical activity in the nerve. In fact, Fig. 7.4 shows that the relative power at the lower CO_2 levels is as great or greater than the relative power associated with higher levels of CO_2 producing phasic respiration.

7.4 Conclusion

The discussion of the muscle waveform power characteristics in Sec. 7.2 suggests that at least two mechanisms, or two different dynamic operators are associated with the respiratory system response to various CO_2 states. The change from one operator to the other occurring at that level of CO_2 at which phasic respiration ceases and apnea begins. It also appears likely that the affect of the dynamic operators state on the muscle waveform during phasic respiration is to produce a linearly related muscle waveform bandwidth and relative power.

The abrupt changes in the nerve waveform power characteristics discussed in Sec. 7.3 also imply the existence of two mechanisms, or two different dynamic operators associated with CO_2 dynamic operators state and its affect on the respiratory nerve electrical activity. For phasic respiration, the most significant factor the state of the dynamic operator has on the nerve waveform is its relative power content. The relative power content increasing as the CO_2 level decreases.

7.5 Recommendations for Further Research in this Area

The next step in the continuing study of nerve and muscle behavior in the respiratory system should be done with the correlation functions defined in Chapter V. The results of which, through the analysis of Sec. 5.8, can lead to a mathematical model of the respiratory system using the model derived in Chapter III. The first model should try to account for the observed respiratory amplitude changes produced by various states of the dynamic operators. After this is done a model producing waveforms similar in bandwidth and relative power to those in this thesis might be produced by a digital-analog computer facility.

The apparent relationship between the state of the CO_2 dynamic operator and the nerve-muscle waveform descriptors mentioned previously leads to an exciting idea suitable for further investigation. Physiologists have been seeking a way to characterize electrical activity of the muscle under tension according to the amplitude, shape, and frequency of occurance of individual muscle cell potentials. The integrated result of many muscle cells firing under controlled levels of tension is identical to the muscle waveform recorded in this experiment.

Therefore, since the state of the CO_2 dynamic operator controls muscle tension, and waveforms similar to those analysed in this experiment represent the combined effect of the individual potentials (whose character is to be described), can the spectra descriptors i.e., bandwidth and relative power be used

for this purpose? This is an intriguing question and when answered would greatly increase the knowledge of muscle action.

Hardware for the digital-analog system interface was part of the effort of this thesis. Therefore, research in the future can be directed to higher theoretical levels and more sophisticated models of the respiratory system. Above all, it is highly recommended that many more experiments be performed to confirm the conclusions of this thesis and to open avenues to the study of the respiratory system that are not dreamed of now.

BIBLIOGRAPHY

1. Blackman, R.B., and J.W. Tukey. The Measurement of Power Spectra. New York: Dover Publications, 1958.

2. Cochran, W.T., J.W. Cooly, et al. "What is the Fast Fourier Transform?" Proceedings of the Institute of Electrical and Electronics Engineers, October 1967, 55: 1664 - 1674.

3. Davenport, William B., and William L. Root. Random Signals and Noise. New York: McGraw-Hill Book Co., 1958.

4. DeWet, Pieter Daniel. "Anatomical and Physiological Investigations of the Avian Respiratory Muscles" (Ph.D. dissertation, University of Minnesota, 1966).

5. Digi-Data Corporation. Operation and Maintenance Manual DSR 1400 Series Digital Stepping Recorders. Hyattsville, Md. : Digi-Data Corp.

6. Frandson, R.D. Anatomy and Physiology of Farm Animals. Philadelphia: Lea and Febiger, 1965.

7. Goodman, Lester. "Oscillatory Behavior of Ventilation in Resting Man." Institute of Electrical and Electronics Engineers on Bio-Medical Engg., July , 1964, BME-11: 82-93.

8. International Business Machines Corporation (IBM). IBM Application Program: System 1360 Scientific Subroutine Package (360A-CM-03X) Version II Application Description. H20-0166-4. White Plains, New York: IBM, 1967.

9. IBM. IBM Field Engineering Manual of Instruction 2401, 2402, 2403, 2404 Magnetic Tape Units Models 1, 2, and 3. Form 223-2819-1. Poughkeepsie, New York: IBM, 1965.

10. IBM. IBM System 1360 Component Description 2400-Series Magnetic Tape Units and 2816 Switching Unit. Form No. A22-6866-3. Poughkeepsie, New York: IBM, 1966.

11. IBM. IBM 2400 Magnetic Tape Units Original Equipment Manufacturers Information. Form No. A22-6862-3. Poughkeepsie, New York: IBM, 1966.

12. Laudau, H.J. "Sampling, Data Transmission, and The Nyquist Rate." Proceedings of the Institute of Electrical and Electronics Engineers, October, 1967, 55: 1701-1706.

13. Lee, Y.W. Statistical Theory of Communication. New York: John Wiley and Sons, 1960.

14. Parsons, Donald. "A Theoretical Analysis of the Sample Statistics for Evoked Cortical Rsponses" (M.S. thesis, Washington University Severz Institute of Technology, 1963).

15. Precision Instrument. Instruction Manual Portable Instrumentation Tape Recorder Model PI-6100. Manual No. PI-M-6100.

16. Schwartz, Mischa. Information Transmission, Modulation, and Noise. New York: McGraw-Hill Book Co., 1959.

17. Texas Instruments, Inc., Apparatus Division. Model 848 AD Converter with Multiplexer. Manual No. 178766-0001. Houston, Texas: Texas Instruments, 1967.

18. Texas Instruments, Inc., Apparatus Division. Model 854-DIC-03A-2 Digital - Analog Converter. Manual No. 185580. Houston, Texas: Texas Instruments, 1967.

19. United States Air Force. SM68 Missile Weapon System Radio-Inertial Guidance System Computer. T.O. 21-SM68 -2F-6-1. St. Paul, Minn.: Air Force, 1963.

APPENDIX A

ANALOG-TO-DIGITAL CONVERSION SYSTEM

A.1 Introduction

This appendix includes the majority of work done on the design and development of the analog-to-digital conversion system. The data processing system represents the majority of work, time, and effort in the realization of this thesis. At the time of its conception a need for analog-to-digital conversion was desperately needed by several departments at Kansas State University. Addition of an IBM 360/50 at the university computing center opened the door to extensive and sophisticated analysis of experimental data. Unfortunately, almost all experimental data was analog in nature and not compatible with digital computer input processes (e.g., nerve and muscle signals).

Another area where a data conversion system was needed was in the Department of Psychology. They were involved in a human tracking experiment. It was found that hand scoring of raw analog data varied widely according to the individual scoring a particular experiment. Besides this, handscoring was a laborious task involving at least one afternoon to score only one trial of an experiment. Obviously, something had to be done. The data processing system described herein was, in part, a solution to their problems. For further information on this subject see Dale E. Bentrup's Master's thesis, Kansas State University, June 1, 1968. Using this system Bentrup has reduced the

scoring time to a minimum and greatly enhanced the reliability of the experimental results. In fact, he can now score the same number of trials in one afternoon that would have taken a month to score by hand.

This writer's interest was in the application of information theory and statistics to biological data analysis. Data was available to work with, but it was in analog form, and not suitable for computor methods of analysis. The following sections therefore include the design and development of a data processing system that enabled the theoretical work to commence.

A.2 Analog-to-Digital Converter Output Number System

The combination multiplexer and analog-to-digital converter (ADC) used in the system is a Series 848 ADC built and purchased from Texas Instruments. It operates in straight binary format. It's output format is either offset binary or twos complement.

An offset binary system is defined as,

+ full scale = 1 1111 1111 1111 1

zero = 1 0000 0000 0000 0

- full scale = 0 0000 0000 0000 0

and a twos complement number system is defined as,

+ full scale = 0 1111 1111 1111 1

zero = 0 0000 0000 0000 0

- full scale = 1 0000 0000 0000 0

Notice the only difference between the offset binary and twos complement number system is that the sense of the

sign bit is reversed in the twos complement system. The offset binary system option was chosen to facilitate the reconstruction of the sampled voltage in the IBM 306/50.

For the offset binary system the input voltage can be reconstructed from the binary output bits with the formula,

$$e_i = \frac{1}{E_{fs}} \left\{ \left(\sum_{j=1}^{n} \frac{A_k}{2^n} \right) - 1 \right\} \qquad (A.1)$$

where, e_i = input voltage

E_{fs} = machine full-scale voltage 10V

n = number of output bits 13

A_k = binary output bits (A_o = sign bit).

The resolution of the data conversion system is equal to the minimum voltage level discernable in the binary output. In this case, the minimum voltage discernable corresponds to the value of the LSB, where,

$$LSB = \frac{E_{fs}}{2^{13}} \qquad (A.2)$$

E_{fs} is 10 volts in the Series 848 ADC so that,

$$LSB = .001247 \text{ V} \qquad (A.3)$$

The accuracy of voltage resolution is approximately one thousandth of a volt as can be seen in Eq. A.3.

A.2.1 Multiplexer Operation

Incorporated in the same package as the ADC is a multiplexer capable of switching up to 16 analog signal

inputs to a single output. The switching sequence is selectable and may be in either of two normal operating modes, sequential or addressable. In the sequential mode, input channels are sampled by internal clock circuitry or are sampled at a rate determined by external equipment. In the addressable mode, input channels may be sampled in any desired sequence controlled by a seven-bit channel address from external equipment (Texas Instruments, pp. 1-3).

In the addressable mode, an address can be entered only when the front panel switch "mode" is in the addressable position and the "clock" switch is in EXT (external). This places the instrument in addressable mode and turns timing control over to external equipment. An address is entered by providing the desired binary address at the proper input pins and then providing a -6V pulse of at least two-microseconds duration at the address set input pins (Fig. A.4). When the address has been set (1.5 μsec. after receiving an address set command) an internally generated -6V pulse is generated and gated to the clock output pin (Fig. A.4).

A.2.2 Analog-to-Digital Conversion

The clock pulse occurring after the address has been set is connected to the "sample initiate" command input pin (Fig. A.4). This clock pulse begins the conversion process. The clock pulse closes an input gate applying the input signal to a holding capacitor through a buffer

stage. The input signal is sampled for 11 μsec. and then the input gate opens leaving the input signal trapped on the holding capacitor.

The held signal is applied as one input to a differential comparator. The second input is taken from an internal precision voltage supply. The internal supply produces an output voltage directly proportional to the binary number contained on the output pins. Thus, if the contents of the binary output pins are manipulated so the two inputs to the differential comparator are equal (i.e., the comparator output is zero), then the binary number on the output pins is directly proportional to the input signal stored on the holding capacitor. The technique used to manipulate the output binary bits to represent the held voltage is called the successive approximation technique. An excellent discussion of this technique is found on page 3-13 of The Texas Instruments instruction Manual No. 178766-0001, Series 848 ADC Manual. Thirty-nine μsec. are required for the successive approximation of the held signal. At the end of this period the output bits are available to external equipment (Fig. A.3) as a parallel 14 bit display.

Basically, four events must occur for conversion:

1. Analog signals connected to multiplexer inputs
2. Channel address entered in multiplexer
3. Address set command pulse transmitted to multiplexer

4. Clock pulse routed to sample initiate command input. The binary output appears 39 μsec. after initial address set command.

A.2.3 Electrical Specifications of ADC Control Signals

The specifications are tabulated in table A.1 below.

Multiplexer	
Number of input channels	16
Signal Input	$\pm$ 10 volts
Logic levels	1 = 6V, 0 = 0 Volts
Channel Address	seven-line, single rail, binary address
Address set command	external clock
Clock (internal)	-6V pulse occurring 1.5 μsec. after address set command
Input impedence	$\geq$ 100MΩshunted by $\leq$ 25pf
Maximum source impedence	1000 Ω
Analog-to-Digital Convertor	
Total system cycle time	39 μsec.
Parallel digital output	single rail, 14 bits
Control Signal Requirements	
Rise time	$\leq$ .5 μsec.
Pulse duration	$\geq$ 2 μsec.
Fall time	$\leq$ .5 μsec.
Maximum current	+ 2.0 ma

TABLE A.1. Electrical specifications of ADC

A.3 Digital Stepping Recorder (DSR)

The digital stepping recorder used in the data processing system is a Precision Instruments DSR 1420. Its general specifications are as listed in table A.2. Electrical specifications are listed in table A.3. (Digi. Data Corp.)

1.	Recording Rate	200 characters/sec.
2.	Interrecord Gap	<130 ms
3.	Tape Width	½ inch standard
4.	Number of Tracks	7
5.	Interrecord Gap Generation	3/4 inch (under ext. control)
6.	Bit Density	200 BPI
7.	Parity	longitudinal and lateral selectable odd or even
8.	End of File Gap and Mark	3.4 inch (controlled from front panel)
9.	Tape Load Point Positioning	Photocell

TABLE A.2 General specifications of DSR

1.	Signal Inputs	Binary 1 = >-6V, Binary 0 = 0V
2.	Data Inputs	7 lines, must be present during stop-record cmd. pulse; 7.5K impedance
3.	Step-Record Command	50-100 μsec. negative pulse; 7.5K impedance
4.	Interrecord Gap Command	20 μs negative pulse, 15K impedance

TABLE A.3 Electrical Specifications DSR

8.3.1 Operation of the DSR 1420

Operation is very simple. Seven lines of parallel data

are brought to the recorder input (Fig.A.9). A negative pulse of approximately 80 μsec. is applied to the step record input. This automatically writes the input and advances the tape. The one limitation that can not be exceeded is the synchronous digital stepping rate i.e., 200 steps/sec. Exceeding this by a large factor would be disasterous to the stepping mechanism.

A.4 Wiring Diagrams Rack Mounted Analog-to-Digital Converter and Digital-to-Analog Converter

To facilitate operation, the ADC unit was mounted in an upright rack (Fig.A.1) along with a companion Digital-to-Analog-Converter DAC. The DAC was not used in the data processing system described in this thesis. It is anticipated that it will be useful at a later date as a link between the ATHENA digital computer and an analog computer. Therefore, this section will include all wiring documentation of the rack mounted ADC and DAC.

All electrical signals on unit chassis connectors J117, J118, and J119C of the ADC and those on J116 of the DAC were brought to Junction Box 2. J-Box 2 is located at the bottom of the rack and easily accesible to underfloor wiring and cabling (Fig. A.2). Both units can be completely controlled by external equipment.

A number of test and monitor signals were brought to special panels on the front of the rack from the ADC and DAC. Refer to Figs. A.3-A.10 for specific definition

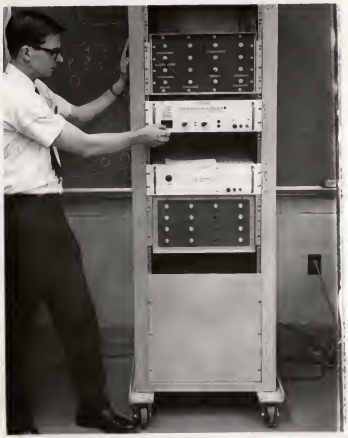

Fig. A.1. Rack mounted analog-to-digital converter and digital-to-analog converter with external connection panels

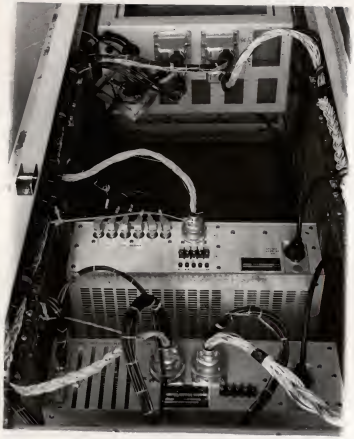

Fig. A.2. Rear view of wiring and connectors inside chassis

of these signals. Note that only two ADC analog input channels (zero and one) are brought to the upper front panel in Fig. A.1. These are especially useful for digitazation from external sources with only one or two channels. Otherwise, the analog inputs on J36 (Fig.A.2) must be used.

A.5 The Digital Computer and Program for Analog-To-Digital Tape Conversion

The computer used to control all peripheral data conversion equipment was a USAF Model SM 68 Missile Weapon System semi-general purpose digital computer. It was built by Remington Rand Univac for use in the Titan missile base at Lowry Air Force Base in Denver, Colorado.

When the site was deactivated by the Air Force the computer was obtained by the Department of Electrical Engineering at Kansas State University. At the University the SM 68 Missile computer is called the Athena. Athena has a relatively small memory of 256 twenty-four bit words. A magnetic drum storage section is available which may store up to 8192 seventeen bit words. The drum storage provides permanent storage for program instruction and constants.

Once a program is started it proceeds sequentially through the 8192 addresses, excuting each instruction before preceding to the next address. The minimum time for one instruction to be excuted is 40 μsec. For more information about the programming and operation of Athena

refer to the AF Technical Manual AF04(645)-20 and AF04 (694)-71 titled, SM 68 Missile Weapon System Radio-Inertia Guidance System Computor. The following sections will assume a knowledge of sections V, VI, VII, VIII, IX, and X of the technical manual. These sections include computer control, arithmetic, magnetic core storage, magnetic drum storage, programming instructions, and input-output data routing. All instructions in the following sections are given in octal code as are all drum addresses and constants stored in core locations.

A.5.1 Input-Output Signals and Bit Positions On Control Console

The data conversion system requires four command signals from the Athena computer. They consist of:

1. a multiplexer address in straight binary code
2. an address set command for the multiplixer
3. a step-record command for the digital tape deck
4. an end of record command for the digital tape deck.

In addition, Athena must act as a buffer for the 14 binary bit ADC output. Figs. A.3 - A.10 are wiring diagrams showing the connections of the peripheral equipment with the Athena computer. Fig. A.11 is a listing of the computer registers as they appear on the control console with the corresponding four command signals and 14 bit binary sample inputs. Figs. A.12 and A.13 display the wiring cables at the Athena mating connector and C-Box 80300.

P117- 1	Sign		J36-1
2	Sign		J36-2
3	Bit 1		NC
4	Bit 1		J36-5
5	Bit 2		NC
6	Bit 2		J36-7
7	Bit 3		NC
8	Bit 3		J36-9
9	Bit 4		NC
10	Bit 4		J36-11
11	Bit 5		NC
12	Bit 5		J36-13
13	Bit 6		NC
14	Bit 6		J36-15
15	Bit 7		NC
16	Bit 7		J36-17
17	Bit 8		NC
18	Bit 8		J36-19
19	Bit 9		NC
20	Bit 9		J36-21
21	Bit 10		NC
22	Bit 10		J36-23
23	Bit 11		NC

P117-24	Bit 11		J36-25
25	Bit 12		NC
26	Bit 12		J36-27
27	Bit 13		NC
28	Bit 13		J36-29
29	Bit 14		NC
30	Bit 14		J36-31
31	NC		NC
32	NC		NC
33	NC		NC
34	NC		NC
35	Digit Complete		TB1-1
36	Digit Complete		NC
37	Pulse Width		TB1-2
38	Pulse Width		NC
39	Aperture Control		TB1-3
40	NC		NC
41	NC		NC
42	NC		NC
43	AD Low		TB1-4
44	AD High		TB1-5
45	NC		NC
46	Ground		Sheilds

Fig.A.3. Wiring assignments for connector P117 on ADC

P118- 1	NC		NC
2	2^6		J35-1
3	2^5		J35-3
4	2^4		J35-5
5	2^3		J35-7
6	2^2		J35-9
7	2^1		J35-11
8	2^0		J35-13
9	NC		NC
10	2^6		J35-15
11	2^5		J35-17
12	2^4		J35-19
13	2^3		J35-21
14	2^2		J35-23

P118-24	Frame Output		TB4-11
25	Mode Select Cmnd		TB4-4
26	NC		NC
27	NC		NC
28	NC		NC
29	NC		NC
30	NC		NC
31	NC		NC
32	NC		NC
33	NC		NC
34	NC		NC
35	NC		NC
36	NC		NC
37	NC		NC

15	2^1 ···J35-25	38	NC ···NC
16	2^0 ···J35-27	39	NC ···NC
17	Address Set Rdy ···TB4-7	40	NC ···NC
18	Address Set Cmnd ···TB4-1	41	NC ···NC
19	Sample In. Rdy ···TB4-8	42	NC ···NC
20	Sample In. Cmnd ···TB4-2	43	NC ···NC
21	Mode Cnfrm. Output ···TB4-9	44	NC ···NC
22	Ext. Reset Cmnd ···TB4-3	45	NC ···NC
23	Clock Output ···TB4-10	46	Logic Ground ···TB4-6

Fig.A.4. Wiring assignments for connector P118 on ADC

P119C-	1 ····· Channel	0	·····TB3-10
	2 ·····	1	·····TB3-11
	3 ·····	2	·····J37-5
	4 ·····	3	·····J37-7
	5 ·····	4	·····J37-9
	6 ·····	5	·····J37-11
	7 ·····	6	·····J37-13
	8 ·····	7	·····J37-15
	9 ·····	8	·····J37-17
	10 ·····	9	·····J37-19
	11 ·····	10	·····J37-21
	12 ·····	11	·····J37-23
	13 ·····	12	·····J37-25
	14 ·····	13	·····J37-27
	15 ·····	14	·····J37-29
	16 ·····	15	·····J37-29
	17 ····· Common		·····TB3-9
	18 ····· Common		·····TB3-9
	19 ····· Common		·····J37-33

Fig.A.5. Wiring assignments for connector P119C on ADC

P117-35	TB1-1	J36-33&TB2-1	
37	2	J36-35&TB2-2	
39	3	J36-37&TB3-1	
43	4	J36-39&TB3-2	
44	5	J36-41&TB3-3	
46	6	J36-43	
NC	7	NC	
NC	8	NC	
NC	9	NC	
NC	10	NC	
NC	11	NC	

TB1-1	TB2-1	J31	
TB1-2	2	J32	
TB4-7	3	J26	
TB4-8	4	J27	
TB4-9	5	J28	
NC	6	NC	
TB4-10	7	J29	
TB4-11	8	J30	
NC	9	NC	
NC	10	NC	
NC	11	NC	

TB1-3	TB3-1	J23	
TB1-4	2	J24	
TB1-5	3	J25	
TB4-1	4	J19	
TB4-2	5	J20	
NC	6	NC	
TB4-3	7		
TB4-4	8	J22	
P119C-17	9	P119C-18	
P119C-1	10	J37-1&J33	
P119C-2	11	J37-3&J34	

P118-18	TB4-1	J35-29&TB3-4	
P118-20	2	J35-31&TB3-5	
P118-22	3	J35-33&TB3-7	
P118-25	4	J35-33&TB3-8	
NC	5	NC	
P118-46	6	J35-37	
P118-17	7	J35-39&TB2-3	
P118-19	8	J35-40&TB2-4	
P118-21	9	J35-41&TB2-5	
P118-23	10	J35-42&TB2-7	
P118-24	11	J35-43&TB2-8	

Fig.A.5. Wiring assignment for terminal boards in J-Box 1

J35-1	2^6	P118-2	
2	NC	NC	
3	2^5	P118-3	
4	NC	NC	
5	2^4	P118-4	
6	NC	NC	
7	2^3	P118-5	
8	NC	NC	
9	2^2	P118-6	
10	NC	NC	
11	2^1	P118-7	
12	NC	NC	
13	2^0	P118-8	

J35-24	NC	NC	
25	2^1	P118-15	
26	NC	NC	
27	2^0	P118-16	
28	NC	NC	
29	Add.Set Cmnd	TB4-1	
30	NC	NC	
31	Sample In Cmnd.	TB4-2	
32	NC	NC	
33	Ext.Reset Cmnd	TB4-3	
34	NC	NC	
35	Mode Set Cmnd	TB4-4	
36	NC	NC	

14 ... 2^0 ... NC		37 ... Logic Ground ...	TB4-6
15 ... 2^6 ... P118-10		38 ... NC ...	NC
16 ... NC ... NC		39 ... Add.Set Ready ...	TB4-7
17 ... 2^5 ... P118-11		40 ... Sample In.Rdy. ...	TB4-8
18 ... NC ... NC		41 ... Mode Confirm ...	TB4-9
19 ... 2^4 ... P118-12		42 ... Clock Output ...	TB4-10
20 ... NC ... NC		43 ... Frame Output ...	TB4-11
21 ... 2^3 ... P118-13		44 ... NC ...	NC
22 ... NC ... NC		45 ... NC ...	NC
23 ... 2^2 ... P118-14			

Fig.A.6. Wiring assignments for J35 on J-Box 2

J36-1 ... Sign ... P117-1		J36-24 ... NC ...	NC
2 ... NC ... NC		25 ... Bit 11.. P117-23	
3 ... Sign ... P117-2		26 ... NC ...	NC
4 ... NC ... NC		27 ... Bit 12.. P117-25	
5 ... Bit 1... P117-3		28 ... NC ...	NC
6 ... NC ... NC		29 ... Bit 13.. P117-27	
7 ... Bit 2... P117-5		30 ... NC ...	NC
8 ... NC ... NC		31 ... Bit 14...P117-29	
9 ... Bit 3... P117-7		32 ... NC ...	NC
10 ... NC ... NC		33 ...Dig.Compl.TB1-1	
11 ... Bit 4... P117-9		34 ... NC ...	NC
12 ... NC ... NC		35 ... Sample Pulse Width	TB1-2
13 ... Bit 5... P117-11		36 ... NC ...	NC
14 ... NC ... NC		37 ... Aperture Cntr ...	TB1-3
15 ... Bit 6... P117-13		38 ... NC ...	NC
16 ... NC ... NC		39 ...AD Low...	TB1-4
17 ... Bit 7... P117-15		40 ... NC ...	NC
18 ... NC ... NC		41 ...AD High..	TB1-5
19 ... Bit 8... P117-17		42 ... NC ...	NC
20 ... NC ... NC		43 ...Ground...	TB1-6
21 ... Bit 9... P117-19		44 ... NC ...	NC
22 ... NC ... NC		45 ... NC ...	NC
23 ... Bit 10.. P117-21			

Fig.A.7. Wiring assignments for connector J36 on J-Box 2

J37-1.....	TB3-10
2.....	NC
3.....	TB3-11
4.....	NC
5.....	P119C-3
6.....	P119C-6
7.....	P119C-7

Note: The remaining pins (8-45) on J37 are not connected.

Fig.A.8. :Wiring Assignments for connector J37 on J-Box2

J38-1	...	Bit 0	...	P116-1	J38-24	... NC ...	NC
2	...	Bit 1	...	P116-2	25	... NC ...	NC
3	...	Bit 2	...	P116-3	26	... NC ...	NC
4	...	Bit 3	...	P116-4	27	... NC ...	NC
5	...	Bit 4	...	P116-5	28	... NC ...	NC
6	...	Bit 5	...	P116-6	29	... NC ...	NC
7	...	Bit 6	...	P116-7	30	... NC ...	NC
8	...	Bit 7	...	P116-8	31	..Ch.1GND.	P117&J1
9	...	Bit 8	...	P116-9	32	..Ch.1 Out	P117&J1
10	...	Bit 9	...	P116-10	33	..Ch.2GND.	P118&J2
11	...	Bit 10	...	P116-11	34	..Ch.2 Out	P118&J2
12	...	Bit 11	...	P116-12	35	..Ch.3GND.	P119&J3
13	...	Bit 12	...	P116-13	36	..Ch.3 Out	P119&J3
14	...	Bit 13	...	P116-14	37	... NC ...	NC
15	...	NC	...	NC	38	..Ch.4Gnd.	P120&J4
16	...	Common	...	P116-16	39	..Ch.4 Out	P120&J4
17	...	Common	...	P116-17	40	..Ch.5Gnd	P121&J5
18	...	Ext.Ref.	..	P116-18	41	..Ch.5 Out	P121&J5
19	...	Ext.Ref.Gnd.		P116-19	42	..Ch.6Gnd	P122&J6
20	...	Reg.Set Ch.1	...	P116-20	43	..Ch.6 Out	P122&J6
21	...	Reg.Set Ch.2	...	P116-21	44	... NC ...	NC
22	...	Reg.Set Ch.3	...	P116-22	Note:J1-J6 are on the front panel.		

Fig.A.9. Wiring Assignments for P116 on the DAC and J38 on J-Box2

Athena Plug-Pin Number	Athena Logic Name	J80300 Terminal Board Assignments	ADC Wiring Assignments
P10105-41	...Acc.R-06	TB3-40	NC
42	...Acc.R-07	TB4-41	NC
43	...Acc.R-08	42	NC
44	...Acc.R-09	43	NC
45	...None	44	NC
46	...None	NC	NC
47	...	TB4-45	NC
48	...Targ.Ident.Cont.1..	46	NC
49	...Common	NC	NC
50	...Targ.Ident.Cont.2.	TB4-47	NC
51	...Common	NC	NC
52	...Miss.Distance Cont..	TB4-48..	NC
53	...Common	TB7-79	Ground
54	...Plotting BD Cont.	TB4-49	NC
55	...Common	TB7-80	Ground
56	...PB Reby Gnd...	TB4-50	NC
57	...Common	NC	NC
P10205-1	...Disc.R-02	TB5-51	DSR-21
2	...Disc.R-10	52	NC
3	...Disc.R-11	53	P35-29
4	...Disc.R-12	54	NC
5	...DR-00	55	NC
6	...DR-01	56	NC
7	...DR-02	57	NC
8	...DR-03	58	NC
9	...DR-04	59	NC
10	...DR-05	60	NC
11	...DR-06	TB6-61	NC
12	...DR-07	62	NC
13	...DR-08	63	NC
14	...DR-09	64	NC
15	...DR-10	65	NC
16	...DR-11	66	NC
17	...DR-12	67	NC
18	...DR-13	68	NC
19	...DR-14	69	NC
20	...DR-15	70	NC
21	...DR-16	TB7-71	NC
22	...DR-17	72	NC
23	... NC	NC	NC
24	...DR-18	TB7-73	NC
25	...DR-19	74	NC
26	...DR-20	75	NC
27	...DR-21	76	NC
28	...DR-22	77	NC
29	...DR-23	78	DSR

Athena Plug-Pin Number	Athena Logic Name	J80300 Terminal Board Assignments	ADC Wiring Assignments
P10105-1	...BDR-00 ...	TB0-1 ...	P36-29
2	...BDR-01 ...	2 ...	27
3	...BDR-02 ...	3 ...	25
4	...BDR-03 ...	4 ...	23
5	...BDR-04 ...	5 ...	21
6	...BDR-05 ...	6 ...	19
7	...BDR-06 ...	7 ...	17
8	...BDR-07 ...	8 ...	15
9	...BDR-08 ...	9 ...	13
10	...BDR-09 ...	10 ...	11
11	...BDR-10 ...	TB1-1 ...	9
12	...BDR-11 ...	2 ...	7
13	...BDR-12 ...	3 ...	5
14	...BDR-13 ...	4 ...	3
15	...BDR-14 ...	5 ...	NC
16	...BDR-15 ...	6 ...	NC
17	...BDR-16 ...	7 ...	NC
18	...BDR-17 ...	8 ...	NC
19	...BDR-18 ...	9 ...	NC
20	...BDR-19 ...	10 ...	NC
21	...BDR-20 ...	TB2-21 ...	NC
22	...BDR-21 ...	22 ...	NC
23	...None ...	NC ...	NC
24	...BDR-22 ...	TB2-23 ...	NC
25	...Pitch Data 1.	24 ...	P35-13
26	...Pitch Data 2.	25 ...	P35-11
27	...Pitch Data 3.	26 ...	P35-9
28	...Pitch Data 4.	27 ...	P35-7
29	...Pitch Sign...	28 ...	NC
30	...Yaw Data 1...	29 ...	NC
31	...Yaw Data 2...	30 ...	NC
32	...Yaw Data 3...	TB3-31 ...	NC
33	...Yaw Data 4...	32 ...	NC
34	...Yaw Sign ...	33 ...	NC
35	...Acc.R-00 ...	34 ...	DSR-4
36	...Acc.R-01 ...	35 ...	DSR-5
37	...Acc.R-02 ...	36 ...	DSR-6
38	...Acc.R-03 ...	37 ...	DSR-7
39	...Acc.R-04 ...	38 ...	DSR-8
40	...Acc.R-05 ...	39 ...	DSR-9

Fig.A.9.1. Wiring assignments for J-Box J80300 located under floor of Athena Computor

(Continued Fig.A.9.)

Athena Plug-Pin Number	Athena Logic Name	J80300 Terminal Board Assignments	ADC Wiring Assignments
P10205-30	...DR-24	... TB8-81 ...	NC
31	...DR-25	... 82 ...	NC
32	...DR-26	... 83 ...	NC
33	...DR-27	... 84 ...	NC
34	...DR-28	... 85 ...	NC
35	...Display Common	... 86 ...	NC
36	...TI Display-00	... 87 ...	NC
37	... -01	... 88 ...	NC
38	... 02	... 89 ...	NC
39	... 03	... 90 ...	NC
40	... 04	..TB9-91 ...	NC
41	... 05	... 92 ...	NC
42	... 06	... 93 ...	NC
43	... 07	... 94 ...	NC
44	...TI Display-08	..TB9-95 ...	NC
45	...TI Display-09	..TB9-96 ...	NC
46	... NC	... NC ...	NC
47	...TI Display-10	..TB9-97 ...	NC
48	... 11	... 98 ...	NC
49	... 12	... 99 ...	NC
50	... 13	... 100 ...	NC
51	... 14	.TB10-101 ...	NC
52	... 15	... 102 ...	NC
53	... 16	... 103 ...	NC
54	... 17	... 104 ...	NC
55	... 18	... 105 ...	NC
56	... 19	... 106 ...	NC
57	...Burnout	... NC ...	NC
58	...Ground	... NC ...	NC
59	...PB Relay Ground	.TB10-107 ...	NC
60	...Ground	... NC ...	NC
61	...DISC R-05	..TB10-108 ...	NC
62	...Ground	... NC ...	NC

Fig.A.9.1. Wiring assignments for J-Box J80300 located under floor of Athena Computor

DSR-1	...	Record	...	P301-G
2	...	Step	...	G
3	...	IR Gap	...	H
4	...	IBM Bit 1	...	A
5	...	IBM Bit 2	...	B
6	...	IBM Bit 4	...	C
7	...	IBM Bit 8	...	D
8	...	IBM Bit A	...	E
9	...	IBM Bit B	...	F
DSR-35	...	Ground	...	M

Note: DSR-10 and DSR-13 are shorted together, all other pins on both plug are not connected.

Fig.A.9.2. Digital Stepping Recorder (DSR)-to-Athena Cable

All pins of P300 A and B are wired "one-to-one" to P35 and P36, respectively, except pins P300 B-46 to P300 B-54 which are not connected.

Example: P300B-20 ..... P36-20
P300A-37 ..... P35-37

Fig.A.10. Athena-to-ADC Cable

Computer Console Register	Bit Position Function
steering register bits 00-03	multiplexer binary address
discrete register bit 02	tape step-record command
discrete register bit 10	end of record command
discrete register bit 11	address set command
acceleration register bits 00-15	fourteen bits ADC output

Fig.A.11 Listing of input and output functions and their corresponding Athena computer registers

A.5.2 One Channel Sample 50 Times Per Second Program

This program enables the sampling of one analog data channel approximately 50 times in one second and converting to digital form. The program in machine language with some general comments is given in Fig. A.14. The following sections explain the subroutines in the program. Again, all addresses, core locations, instructions, and constants are given in octal code.

A.5.3 Sample Counting Subroutine

The sample counting subroutine controls the number of samples taken and indirectly the length of the analog signal that can be sampled. The subroutine extends from address 02000-02006 (See Fig.A.14). The first instruction 024007 at address 02000 initializes the control console and is really not part of the counting program. Instruction 060256 at address 02001 begins the counting subroutine. It clears the accumulator by transmitting 0000 0000 from Core Location (CL) 256. Instruction 064255 at address 02002 adds 0000 0001 stored in CL 255 to the cleared

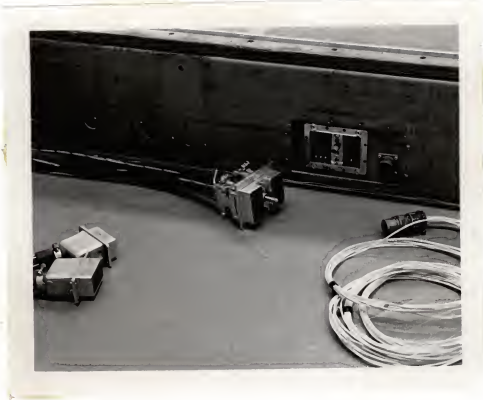

Fig. A.12. Connectors for wiring harness from ADC rack to Athena Computer and wiring harness from the DSR to Athena

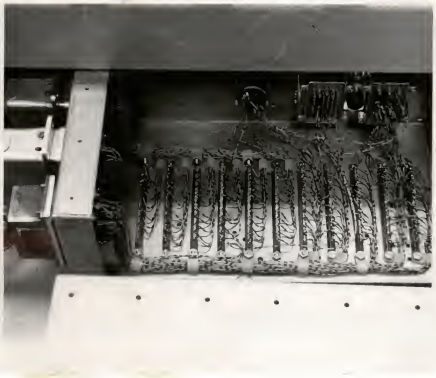

Fig. A.13. J-Box 80300 located under floor of Athena Computer

ADDRESS	INSTRUCTION	COMMENTS
02000	024007	
02001	060256	
02002	064255	(counting program)
02003	004256	
02004	066252	
02005	222007	sign jump
02006	200331	jump to end of run program
02007	020001	
02010	024012	sets multiplexer address
02011	024007	
02012	006031	stores binary
02013	022001	places channel number
02014	024010	
02015	004100	1st step-record
02016	004100	generated
02017	024007	
02020	202175	time delay
		generated
02175	062031	
02176	106016	complements sample and
		clears accumulator
02206	060027	
02207	104004	shifts 1st four bits
		to accumulator
02212	004040	
02213	022040	places bits at tape input
02214	024010	
02215	004100	2nd step-record
02216	004100	pulse generated
02217	024007	
02220	202406	time delay
		generated
02406	104006	
		6 more bits shifted and
02412	004040	placed on tape input
02413	022040	
02414	024010	
02415	004100	3rd step-record
02416	004100	pulse generated
02417	024007	
02420	202606	time delay
		generated
02606	104006	
02612	004040	last 6 bits shifted and
02613	022040	placed at tape input
02614	024010	
02615	004100	4th step-record
02616	004100	pulse generated
02617	024007	
02620	202000	timed jump to beginning
		of program

Fig.A.14. 50 Sample/sec one channel sample program

accumulator. Instruction 004256 stores the accumulator in CL 256. Instruction 066252 at address 02004 subtracts the number in CL 252 from the number in the accumulator. The number in CL 252 is equal to N+1, where N is the number of required samples.

Instruction 222007 at address 02005 is a sign jump. If the quantity in the accumulator is negative and not equal to zero, the next instruction executed is at address 02007. This is the case that exists until N samples have been converted. On the N+1 sample the number in the accumulator is equal to zero. When this happens the sign jump instruction causes the next instruction in sequence to be executed. This instruction is 200331 at address 02006 which is an unconditional jump to the instruction at address 331. At address 331 the End of Run program is stored.

Assuming that a negative number is in the accumulator at the execution of the sign jump instruction (i.e., less than N samples have been converted), instruction 020001 at address 02007 is executed. This instruction transmits to the steering register the sampled channel number stored in CL 1. The number in CL 1 is 7776 7777. Only the low order bits are transmitted to the steering register. True bits are placed on steering register positions 00-05. The pins connected to these positions have the opposite sense of the control console register positions. Therefore, no voltage appears on output pins corresponding to positions

00-05. The steering register is wired to the multiplexer binary address input (Fig.A.9), thereby setting the analog channel to be sampled to zero.

Instruction 024012 at address 0210 (2010) begins the required address set pulse. This pulse must be at least 40 μsec. long and equal to -6V for the digital stepping recorder to start its step-record process. Instruction 024012 transmits 2000 stored in low order core location 12 to the descrete register. This turns off position 11, the address set command bit. This bit exhibits a reverse sense at its output pin connected to the multiplexer (Fig.A.4). Therefore when bit 11 is turned off -6V appears at the multiplexer input. Forty μsec.later, the next instruction 024007 at address 02011 turns on bit 11 turning off the -6V at the multiplexer input.

The ADC completes digitization 39 μsec.after the address set pulse is initiated. Therefore, the next instruction executed can store the 14 bit ADC binary output in core. These 14 bits are shown connected to Athena in Fig.A.3. Instruction 006031 at address 02012 stores the 14 bits is CL 31.

The first step in writing the magnetic tape is to record the channel number on the first tape character as shown in section A.6. Instruction 022001 at address 02013 transfers the channel number to the acceleration bit positions 00-05. Again the corresponding output pins connected to the Digital tape deck's six inputs exhibit reverse sense. Thus, the complement of the channel number

is transmitted to the acceleration register.

A step-record pulse of -6V and longer than 50 μsec. is required to record the first tape character. Instruction 024010 at address 02414 transmits 0004 in CL 10 to the descrete register. Bit position 02 of the discrete register is turned on. The corresponding output pin connected to the step-record input is of the correct sense. The length of this pulse is increased by the two dummy instructions 004100 and 004100 at addresses 02015 and 02016. These instructions store the accumulator's content in CL 100 which in no way affects the program. Instruction 024007 at address 02017 turns of discrete register pin 02 and the -6V applied to the step-record input. The first tape character has now been written.

The next instruction is an unconditional jump required for the synchronous operation of the digital tape deck's stepping motor. The jump instruction is 202175 at address 02020. The next instruction to be executed is at address 02175 and begins the process of writing the second tape character. Instruction 062031 at address 02175 causes the complement of the 14 bit sample store in CL 31 to be transmitted to the accumulator. The complement is transmitted to account for the acceleration reverse sense pins connected to the digital tape deck's six input connectors.

The 14 sample bits are shifted left into the quotient register 14 positions so that the writing process can begin. Instruction 106016 at address 02176 does the shifting. This shifting process takes eight instruction times so that

the next instruction is at address 02206. The instruction is 060027 and transmits 0000 from low order core location 27 to the accumulator which clears the accumulator for the sample writing process.

The 14 complemented sample bits are shifted four positions to the left by instruction 104004 at address 02207. This places the first four of the negative sample bits on accumulator bit positions 00,01,02, and 03. Accumulator bit positions 04 and 05 are of no consequence in this character due to the IBM 360/50 decoding program blanking them out. The contents of the accumulator are stored in CL 40 by instruction 004040 at address 02212. Then the contents of CL 40 are transmitted to the acceleration register by instruction 022040 at address 02213. This places the bits of the second tape character at the proper tape deck input pins and of correct polarity.

The step-record pulse is generated by instructions at addresses 02214, 02215, 02216, and 02217 as previously explained.

A 5ms delay for synchonous tape drive is obtained by the jump instruction 202406 at address 02220. Instruction 104006 at address 02406 shifts the next six complemented sample bits from the quotient register into accumulator bit positions 00-05. Instruction 004040 at address 02412 stores the accumulator contents in CL 40. Instruction 022040 at address 02413 transmits the contents of CL 40 to the acceleration register placing the next six complemented sample bits on acceleration

bit positions 00-05. This places the proper tape inputs for generating the third tape character at the tape deck input. A step-record pulse is generated as described by instructions at addresses 02414, 02415, 02416, and 02417.

Instruction 202606 at address 02420 is a jump required for the synchronous drive of the tape deck. At address 02606, instruction 104006 shifts the remaining complemented sample bits from the quotient register into the accumulator. These four bits are in accumulator bit positions 00, 01, 02, and 03. Bits in positions 04 and 05 are ignored by the IBM 360/50 decoding program. The accumulator contents are stored in CL 40 by instruction 004040 at address 02612. From CL 40 the contents are transmitted to the acceleration register such that the proper complemented sample bits are placed at the digital recorder input connections for writing the fourth and last character. The step-record pulse is generated by instructions at 02614, 02615, 02616, and 02617.

Instruction 202000 at address 02620 is an unconditional jump to the beginning of the sample program and starts the process over again.

A.5.4 End of Run Subroutine

The end of run subroutine places a number corresponding to the trial number placed on the Athena computer constant register. In addition, the next three characters are also written with the run number. This allows the

360/50 computer's decoding program to treat the trail number exactly as if it was a channel number. The remaining characters are treated as if they were a sample and must be ignored by the programmer.

The run number program was written on drum number three in such a fashion so that the tape drive pulses are 5ms apart. In addition, an interrecord gap command is generated 5ms after the run number has been written and sent to the digital tape deck. A listing of this program is given in Fig. A.15 along with some comments.

A.5.5 Load Constant Subroutine

The load constant routine must be run before any attempt at data conversion is begun. This program initializes all core locations used in the counting routine and control bits. It is located on drum number zero between addresses 00141 and 00211. The load constant program is listed in Fig. A.16.

A.6 Definition of Binary Data Magnetic Tape Bit Structure

The seven track 2400 tape units at the Kansas State University computing center have an optional feature which allows the writing and reading of binary data other than Binary Coded Decimal (BCD). This is the feature that allows the ADC digital output to be recorded on magnetic tape with the DSR 1200 stepping recorder and subsequently entered into the IBM 360/50 core for translation to a usable form.

ADDRESS	INSTRUCTION	COMMENTS
06176	060027	initializes counting
06177	004256	routine to zero
06200	060027	clears accumulator
06201	002070	enters run number
06202	004004	
06203	062004	complements run number
06204	004004	
06205	022004	places run number at tape input
06206	024010	
06207	004100	1st step-record
06210	004100	pulse generated
06211	024007	
06212	206406	timing jump delay
06406	024010	
06407	004100	2nd step-record
06410	004100	pulse generated
06411	024007	
06412	206606	timing jumb delay
06606	024010	
06607	004100	3rd step-record
06610	004100	pulse generated
06611	024007	
06612	207006	timing jump delay
07006	024010	
07007	004100	4th step-record
07010	004100	pulse generated
07011	024007	
07012	207206	timing jump delay
07206	017005	interrecord gap
07207	060027	pulse generated
07210	017005	
07211	320040	manual stop

Fig. A.15. Enter run number program

ADDRESS	INSTRUCTION	COMMENTS
141	127776	
142	147777	loads CL 1
143	004001	
144	127775	
145	147776	loads CL 2
146	004002	
147	127774	
150	147775	loads CL 3
151	004003	
152	126000	
153	140000	loads CL 7
154	004007	
155	126004	
156	140000	loads CL 10
157	004010	
160	124000	
161	140000	loads CL 11
162	004011	
163	122000	
164	140000	loads CL 12
165	004012	
166	120000	
167	140000	loads CL 27
170	004027	
171	121751	1751_8 equals N+1
172	140000	
173	004254	samples (controls length of 3 channel program can be varied as required)
174	120001	
175	140000	loads CL 255
176	004255	
177	120000	
200	140000	loads CL 256
201	004256	
202	120004	
203	140000	loads CL 4
204	004004	
205	125671	5671_8 equals N+1
206	140000	
207	004252	(can be changed to control length of 50 s/s program)
210	320004	manual stop
211	200040	jump to 00040

Fig.A.16. Program to load constants

The binary conversion feature is set on by a job control card. This forces the seven track BCD translater off and the tape parity checks to odd. Therefore, the seven track tape is written with odd parity.

The binary code chosen takes advantage of the fact that four tape characters are placed into three bytes of the computor core (IBM, Ref.11). The code was designed so it included the following data,

1. multiplexer address of channel being sampled
2. 14 bit sampled data
3. run number.

Fig.A.17 illustrates how two samples and their corresponding channel numbers appear on the digital magnetic tape. The run number is written in the address location after the required number of samples of data have been converted.

Parity	P	P	P	P	P	P	P	P
B	X	X	D_5	D_{11}	X	X	D_5	D_{11}
A	X	X	D_6	D_{12}	X	X	D_6	D_{12}
8	A_1	D_1	D_7	D_{13}	A_4	D_1	D_7	D_{13}
4	A_3	D_2	D_8	D_{14}	A_3	D_2	D_8	D_{14}
2	A_2	D_3	D_9	X	A_2	D_3	D_9	X
1	A_4	D_4	D_{10}	X	A_1	D_4	D_{10}	X

A = address bit P = parity bit
D = sample bit X = not used

Fig.A.17 Digital tape bit structure definition

A.6.1 IBM 360/50 Assembler Language Decoding Program

The seven track tape unit convertor places the tape characters into the computer core as shown in Fig.A.18 (parity bits are ignored).

$XXA_4A_3A_2A_1XX$	$D_1D_2D_3D_4D_5D_6D_7D_8$	$D_9D_{10}D_{11}D_{12}D_{13}D_{14}XX$
012 3 4 5 67	0 1 2 3 4 5 6 7	0 1 2 3 4 5 67

Core Locations

Fig.A.18. Address and sample bits as they appear in core

The data is in a modified negative radix binary notation with a 1 bit positive and a 0 bit negative. The 360/50 assembler language program was written to separate the data from unused bits and write the data on tape in Fortran acceptable format 10(13,15).

The data translation from negative radix is accomplished by manipulation of the equation for measured voltage reconstruction as follows

$$Vm = E_{fs}\left[\left(\sum_{n=o}^{B}\ \frac{Bn}{2^n}\right)\ -1\right]$$

$$Vm = \frac{E_{fs}}{2^{13}}\left[\left(\sum_{n=o}^{13}\ Bn2^{13}2^{-n}\right)\ -2^{13}\right]$$

$$Vm = \frac{E_{fs}}{2^{13}}\left[\left(\sum_{n=o}^{13}\ 2^{13-n}Bn\right)\ -2^{13}\right].$$

The summation can be evaluated in base 10 by treating the data as if it were a positive radix (base) 2 number and converting to base 10 in the normal manner, as shown in Fig.A.19.

Original Bit	S_0	B_1	B_2	B_3	B_4	B_5	B_6	...	B_{13}					
13-n	13	12	11	10	9	8	7	...	0					
Modified Bit Value	2^{13}	2^{12}	2^{11}	2^{10}	2^9	2^8	2^7	...	2^0					

Fig. A.19. Conversion of negative radix 2 number to base 10

In order to avoid roundoff errors, only the expression in brackets is evaluated and is written as a fixed-point number in 80 column card images in blocked format on a magnetic tape. The remainder of the conversion is done with the user's Fortran program which must convert the five digit integer sample to a real number and multiply by the scale factor 10/1892.

The assembler program is completely general and can be used for any data. Input and output blocksize and tape densities can be varied using the 360/50 job control language recompling the assembler language program. See Fig. A.20 and Fig. A.21 for a flow chart and listing of the assembler convertor program, respectively.

A.6.2 Notes to the Programmer Operator

The length of the analog signal to be converted

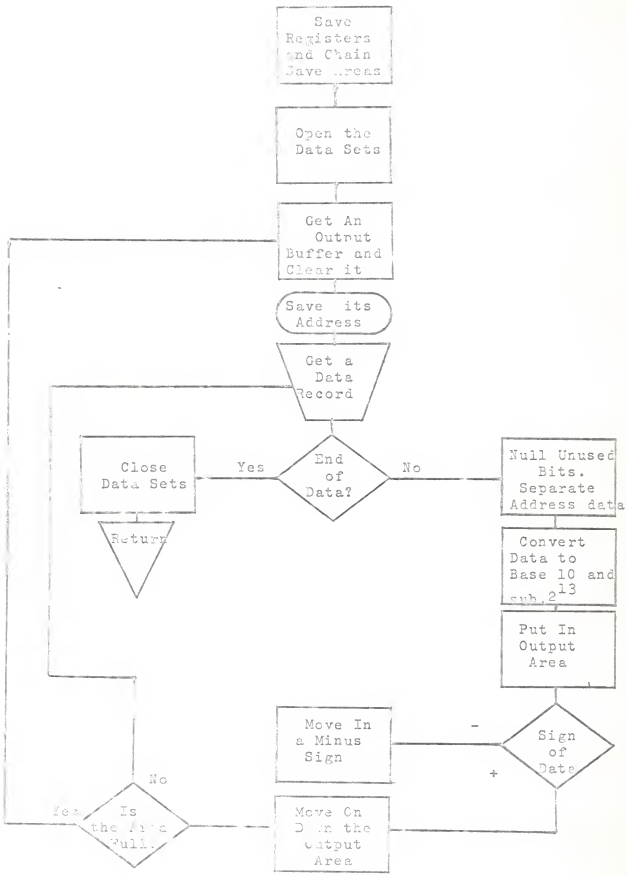

Fig.A.20. Data Conversion Flowchart

```
//ASMBL   EXEC  ASMFCLG,PARM.ASM='LOAD,DECK,LINECNT=55'
//ASM.SYSIN  DD  *
         TITLE 'ATHENA DATA CONVERTER J.P.L.'
CONVRT   START X'E820'                 THIS STATEMENT IS OPTIONAL.
ORG      SAVE  (14,12),,*              SAVE THE REGISTERS.
         LR    11,15                   LOAD THE BASE REGISTER.
         USING ORG,11                  ESTABLISH ADDRESSABILITY.
         ST    13,SAVE+4               STORE HIS SAVEAREA ADDRESS.
         LA    5,SAVE                  GET OUR SAVEAREA ADDRESS.
         ST    5,8(0,13)               STORE IT.
         LA    13,SAVE                 MAKE IT AVAILABLE TO CALLED PROGRAMS.
         OPEN  (INDCB,(INPUT),OUTDCB,(OUTPUT)) OPEN DATA SETS FOR PROC.
PUTDATA  PUT   OUTDCB                  EMPTY A BUFFER AND GET A NEW ONE.
         LR    4,1                     COPY ADDRESS OF BUFFER.
         LA    5,10(0,0)               LOAD 10 INTO REGISTER 5.
         MVI   0(1),C' '               SET UP TO
         MVC   1(131,1),0(1)             CLEAR THE NEW BUFFER TO BLANKS
GETDATA  GET   INDCB,IN+1              GET AN INPUT RECORD.
         NC    IN,=X'003CFFFC'         ZERO THE INPUT AREA EXCEPT GOOD BITS.
         XR    2,2                     CLEAR REGISTER 2.
         L     2,IN                    LOAD THE DATA INTO IT.
         SRDL  2,18                    SHIFT CHANNEL ADDR. TO RIGHT END.
         SRL   3,16                    SHIFT DATA TO RIGHT END.
         CVD   2,DWORD                 CONVERT CHANNEL TO PACKED DECIMAL.
         CI    DWORD+7,X'0F'           FIX THE SIGN FOR UNPACK.
         USING OUT,4                   ADDRESSABILITY FOR THE OUTPUT RECORD.
         UNPK  OUTCHAN,DWORD           UNPACK THE CHANNEL NUMBER.
         CVD   3,DWORD                 CONVERT DATA TO PACKED DECIMAL.
         SP    DWORD,=P'8192'          COMPENSATE FOR DATA SIGN.
         UNPK  OUTDATA,DWORD           UNPACK THE DATA INTO OUTPUT AREA.
         TM    BITS,X'10'              CHECK THE SIGN OF THE DATA.
         BZ    FIXSIGN                 BRANCH IF IT IS PLUS.
         MVI   OUTSIGN,C'-'            OTHERWISE, MOVE IN A MINUS SIGN.
FIXSIGN  CI    BITS,X'F0'              WIPE OUT THE ORIGINAL SIGN.
         A     4,=F'8'                 INDEX DOWN THE OUTPUT AREA.
         BCT   5,GETDATA               LOOP TEN TIMES.
         B     PUTDATA                 WRITE OUT THE COMPLETED RECORD.
         DROP  4
QUIT     CLOSE (OUTDCB,,INDCB)         CLOSE DATA SETS AND WRITE LAST REC.
         L     13,SAVE+4               RELOAD HIS SAVEAREA ADDRESS.
         RETURN (14,12)                RESTORE THE REGISTERS AND QUIT.
INDCB    DCB   DSORG=PS,MACRF=GM,DDNAME=INPUT,RECFM=FB,EODAD=QUIT,      *
               DEVD=TA
OUTDCB   DCB   DSORG=PS,MACRF=PL,DDNAME=OUTPUT,RECFM=FB,                *
               DEVD=TA
SAVE     DC    18F'0'
IN       DS    1F
DWORD    DS    1D
         LTORG
OUT      DSECT
         DS    CL1
OUTCHAN  DS    CL2
OUTSIGN  DS    CL1
OUTDATA  DS    CL4
         ORG   OUT+7
BITS     DS    CL1
         END   ORG
/*
```

Fig.A.21. Computer Listing of Convertor Program

determines the time the sample program must run. The length of the 50 sample/sec one channel program is controlled by the octal number stored in core location 252. The octal number occupies both the high and low order core positions. In Fig.A.14, 5671_8 equals 4001_{10} converted samples. This is stored in the low order positions by instruction 125671 at address 00205. The high order zeros were made zero by instruction 140000. This program must be run after the constants are entered in their proper place in this program for them to be placed in core.

Calculate the number to be placed in CL 252 by converting the analog signal time duration to samples by the conversion factor 50 samples = 1 sec. Usually, the number of samples chosen is an integral multiple of 10 to ease readout of the data at the IBM 360/50. Do not forget to convert the decimal number to octal before entering it into its proper place.

It is a good idea to run the sample program once with the digital tape recorder OFF to check the length of run and to initialize the computor.

The run number is entered on the first two registers of the constant program in OCTAL form.

After all data has been converted punch END OF FILE (EOF) on the front panel of the digital tape recorder.

APPENDIX B

It is desired to show that the Fourier transform of Eq. 5.24,

$$\Phi_{r_o}(\tau) = h_2(t) \ominus \{h_1(t) * [h_1(t) \ominus \phi_{ff}(\tau)]\} \quad , \tag{B.1}$$

is equal to,

$$\Phi_{rs}(j\omega) = H_2(-j\omega) |H_-(j\omega)|^2 \Phi_{pp}(j\omega) \quad , \tag{B.2}$$

where the symbol $\ominus$ means correlation in the aperiodic sense and the symbol * denotes convolution.

The defining equation for the Fourier transofrm of a function f(t) is,

$$F(j\omega) = \int_{-\infty}^{\infty} f(t) e^{-j\omega t} dt \quad , \tag{B.3a}$$

which leads to the equation,

$$F(-j\omega) = \int_{-\infty}^{\infty} f(t) e^{j\omega t} dt \quad . \tag{B.3b}$$

To begin let $g_1(t)$ equal,

$$h_1(t) * [h_1(t) \ominus \phi_{ff}(\tau)] \quad , \tag{B.4}$$

in Eq. B.1. Eq. B.1 written with the substitution indicated by Eq. B.4 is,

$$\Phi_{r_o}(\tau) = h_2(t) \ominus g_1(t) \quad . \tag{B.5}$$

The Fourier transform of $\phi_{rs}(\tau)$ is,

$$\Phi_{rs}(j\omega) = \int_{-\infty}^{\infty}\int_{-\infty}^{\infty} h_2(\nu) g_1(\nu+\tau) d\nu e^{-j\omega\tau} d\tau \quad ,$$

$$= \int_{-\infty}^{\infty} h_2(\nu) e^{j\omega\nu} d\nu \int_{-\infty}^{\infty} g_1(\nu+\tau) e^{-j\omega(\nu+\tau)} d\tau \quad ,$$

which by comparison with Eqs. B.3a and B.3b means,

$$\Phi_{rs}(j\omega) = H_2(-j\omega) G_1(j\omega) \quad . \tag{B.6}$$

The Fourier transform $G_1(j\omega)$ becomes, using the operations indicated by Eq. B.4,

$$G_1(j\omega) = \int_{-\infty}^{\infty}\int_{-\infty}^{\infty} h_1(\sigma) g_2(t-\sigma) d\sigma e^{-j\omega t} dt \quad ,$$

where,

$$g_2(t) = h_1(t) \ominus \phi_{ff}(\tau) \qquad \text{and,}$$

$$G_1(j\omega) = \int_{-\infty}^{\infty} h_1(\sigma) e^{-j\omega\sigma} d\sigma \int_{-\infty}^{\infty} g_2(t-\sigma) e^{-j\omega(t-\sigma)} dt \quad ,$$

which again by comparison with Eqs. B.3 becomes,

$$G_1(j\omega) = H_1(j\omega) G_2(j\omega) \quad . \tag{B.7}$$

Combining Eq. B.7 with Eq. B.6 yields,

$$\Phi_{rs}(j\omega) = H_2(-j\omega) H_1(j\omega) G_2(j\omega) \quad . \tag{B.8}$$

ACKNOWLEDGEMENT

I wish to express my appreciation to my advisor, Dr. Donald Lenhert, Drs. W. W. Koepsel and M. R. Fedde for their advice, understanding and material contributions during the course of this study.

To my wife, who has served as an able assistant and exhibited confidence in me throughout this work, this thesis is dedicated.

VITA

CHARLES M. HIGHTOWER

Candidate for the Degree of

MASTER OF SCIENCE

Thesis: The Analysis of Nerve and Muscle Electrical Waveforms with the Fast Fourier Transform and Correlation Techniques

Major Field: Electrical Engineering

Biographical:

Personal Data: Born in Philadelphia, Pennsylvania, July 1, 1944, the son of Russell L. and Margaret P. Hightower.

Education: Graduated from Canoga Park High School in 1962; received the Bachelor of Science Degree from Kansas State University, in Electrical Engineering, in June, 1964; completed requirements for the Master of Science Degree in June, 1968.

Scholastic Societies, Professional Organizations, and Honors: Graduated Cum Laude from Kansas State University in June, 1966; elected to membership in Phi Kappa Phi, Eta Kappa Nu, and Sigma Tau; participated in Engineering Honors Program during undergraduate work; member Institute of Electronic and Electrical Engineers; completed Engineer-in-Training examination, state of Kansas, 1966.

Professional Experience: Associate Engineer at Douglas Aircraft Company working on Long Tank Thor guidance system from June to September, 1966; from June to September, 1967 was associated with the Space Systems Division of Collins Radio Company; taught undergraduate engineering courses for the Department of Electrical Engineering at Kansas State University as an instructor in 1968.

THE ANALYSIS OF NERVE AND MUSCLE ELECTRICAL WAVEFORMS WITH THE FAST FOURIER TRANSFORM AND CORRELATION TECHNIQUES

by

CHARLES HOWARD HIGHTOWER

B. S., Kansas State University, 1966

AN ABSTRACT OF A MASTER'S THESIS

submitted in partial fulfillment of the

requirements for the degree

MASTER OF SCIENCE

Department of Electrical Engineering

KANSAS STATE UNIVERSITY
Manhattan, Kansas

1968

ABSTRACT

The respiratory system common to a large number of living organisms is dependent on a group of receptors sensitive to blood carbon dioxide (CO_2) content for the manipulation of ventilation. Collectively, these receptors are called CO_2 chemoreceptors. Their specific function is to communicate with the central nervous system and notify it of the blood CO_2 content. The central nervous system through a complex array of nerve bundles then stimulates respiratory muscles to perform the operation of ventilation.

Observation of the electrical activity in the respiratory nerve and muscle systems yields no apparent deterministic relationship between the state of the CO_2 chemoreceptors and the electrical activity (which is mainly stochastic in nature).

The effect of the CO_2 chemoreceptors on respiratory electrical activity in the Gallus Domesticus was investigated in this thesis using techniques of modern communications theory in conjunction with data processing by a large digital computer. Results of this analysis indicated that the effect of the CO_2 chemoreceptors on respiratory electrical activity does manifest itself in two deterministic ways. The first descriptive quantity was found with the Fast Fourier Transform of the nerve and muscle waveforms to be the bandwidth of the electrical waveform. The second quantity was found to be the relative power content of the electrical waveforms as indicated by their cumulative power spectra.

The behavior of these two descriptors suggested that the CO_2 chemoreceptor relationship with the respiratory system is best characterized by two distinct mechanisms. One mechanism predominant during phasic respiration and the other during apnea.

An idealized mathematical model of the respiratory system was constructed and analyzed, showing that the Fourier transform of the nerve-muscle crosscorrelation function is an indicator of the accuracy of such a model.

In addition, a brief examination of aliasing due to waveform digitization at a rate below the Nyquist frequency was made. From the results it was recommended that the waveform digitization rate be increased by a factor of from two to four to lessen possible aliasing perturbations. Other recommendations were made concerning the experimental data recording equipment. Also, further areas of research are discussed based on the findings of this thesis.